

Nonlinear effects in two-layer large-amplitude geostrophic dynamics. Part 2. The weak-beta case

By RICHARD H. KARSTEN AND GORDON E. SWATERS

Applied Mathematics Institute, Department of Mathematical Sciences, and Institute of Geophysical Research, University of Alberta, Edmonton, T6G 2G1, Canada

(Received 6 January 1999 and in revised form 14 January 2000)

This paper is a continuation of our study on nonlinear processes in large-amplitude geostrophic (LAG) dynamics. Here, we examine the so-called weak- β models. These models arise when the intrinsic length scale is large enough so that the dynamics is geostrophic to leading order but not so large that the β -effect enters into the dynamics at leading order (but remains, nevertheless, dynamically non-negligible). In contrast to our previous analysis of strong- β LAG models in Part 1, we show that the weak- β models allow for vigorous linear baroclinic instability.

For two-layer weak- β LAG models in which the mean depths of both layers are approximately equal, the linear instability problem can exhibit an ultraviolet catastrophe. We argue that it is not possible to establish conditions for the nonlinear stability in the sense of Liapunov for a steady flow. We also show that the finite-amplitude evolution of a marginally unstable flow possesses explosively unstable modes, i.e. modes for which the amplitude becomes unbounded in finite time. Numerical simulations suggest that the development of large-amplitude meanders, squirts and eddies is correlated with the presence of these explosively unstable modes.

For two-layer weak- β LAG models in which one of the two layers is substantially thinner than the other, the linear stability problem does not exhibit an ultraviolet catastrophe and it is possible to establish conditions for the nonlinear stability in the sense of Liapunov for steady flows. A finite-amplitude analysis for a marginally unstable flow suggests that nonlinearities act to stabilize eastward and enhance the instability of westward flows. Numerical simulations are presented to illustrate these processes.

1. Introduction

Fronts and their associated currents play an essential role in the dynamics of the world's oceans. A typical physical characteristic of an oceanic front is a large change in the density over a short length scale, and is seen in observations as a concentration of sloped isopycnals. Large open-ocean fronts are created by differential heating and wind stresses and can extend across entire ocean basins (Roden 1975). Coastal currents also take the form of isolated fronts overlying sloping bottom topography. These vary from weaker eastern boundary currents such as the California Current (see Ikeda, Emery & Mysak 1984) to the western boundary currents such as the Kuroshio (see Robinson 1983) and the Gulf Stream (see Bush, McWilliams & Peltier 1995). As well, these currents can be global in scale such as the Antarctic Circumpolar Current or more local phenomena such as the Gaspé current. The variety and importance of

frontal currents makes essential the development and analysis of general models that can examine their dynamics.

Despite the variety of ocean surface fronts, they are largely geostrophic in nature, that is, the velocity is principally determined by pressure gradients and the Coriolis effect (Robinson 1983). Yet, it is the variation from geostrophy, the ageostrophic effects, that determines the existence and form of instabilities. As well, fronts are marked by large-amplitude dynamical deflections in the isopycnals. These large deflections cause relatively large velocities and, thus, the nonlinear advection, particularly in the mass equation, cannot be assumed small. As such, the classic quasi-geostrophic (QG) model, which assumes small isopycnal deflection and thus small velocities, is not applicable (see Pedlosky 1987 for details of the QG model). This has lead many to examine fronts using the primitive equations (see Griffiths, Kilworth & Stern 1982; Killworth 1983; Paldor 1983*a, b*; Killworth, Paldor & Stern 1984; Paldor & Killworth 1987; and Paldor & Ghil 1990). However, the difficulty in examining the primitive equations restricts the simple extension of QG analysis while the generalization of results to include the β -effect or bottom topography and the extension to continuously stratified flows are not trivial (Benilov & Reznik 1996). What is required is a simple, rational theory for large-scale frontal dynamics that approximates the primitive equations in such a manner as to include finite-amplitude isopycnal deflection and the dynamically important ageostrophic effects while preserving leading-order geostrophy.

As discussed in Part 1 (Karsten & Swaters 2000), the search for such a theory lead to the development of the large-amplitude geostrophic (LAG) models (see Cushman-Roisin 1986; Benilov 1992; Cushman-Roisin, Sutyrin & Tang 1992; and Benilov & Reznik 1996). These models assume that the characteristic length scale of the flow exceeds the Rossby deformation radius, allowing for geostrophic flows with large-amplitude deflections (Phillips 1963 and Yamagata 1982). As a simple manifestation of an isopycnal model, the LAG models have the advantage that the vertical resolution is concentrated where the horizontal density gradient is greatest and model surfaces which are the preferred mixing surfaces of the ocean (Chassignet & Cushman-Roisin 1991). Importantly, the LAG models can be generalized to examine continuously stratified flows (Benilov 1993, 1994) and can incorporate the β -plane approximation (see Cushman-Roisin 1986; Cushman-Roisin *et al.* 1992; and Benilov & Reznik 1996) or bottom topography (see Swaters 1991, 1993*b*, 1998*a, b*; Karsten & Swaters 1996*b*; and Karsten 1998). As well, LAG models can include outcropping isopycnals that are difficult to examine within shallow-water equations and impossible within the layered QG formalism.

As we pointed out in Part 1 (see also Benilov 1992 and Benilov & Reznik 1996), the strength of the β -effect greatly affects the mathematical structure of the model equations derived and thereby the dynamical characteristics of the resulting flows described. As the intrinsic length scale associated with the dynamics increases beyond the *Rhines scale*, the β -effect becomes progressively more important and makes a contribution even at leading order to the dynamics. The models corresponding to this limit are referred to as *strong- β* models (Benilov 1992). In Part 1, we developed a general stability analysis for steady solutions to these models. We established two new nonlinear stability theorems and developed a linear and weakly nonlinear instability theory as well as presenting numerical simulations. In particular, we identified a new long-wave–short-wave resonance which is responsible for a transfer of energy to large length scales. We examined the nonlinear evolution of the instabilities associated with vanishing potential vorticity (PV) gradients (see Benilov 1995). We showed that a barotropic instability existed in all models, with nonlinear effects leading to eddy

formation when lower-layer effects were weak and breaking waves when they were strong. We also illustrated the possibility of a growing baroclinic wave if the lower-layer PV gradient vanishes in the thin-upper-layer model. This wave grows to large amplitude but does not result in eddies pinching off from the front. Nevertheless, the instabilities we described in Part 1 were either barotropic in nature or were slowly growing.

On the other hand, smaller-scale, strong-flow currents like those associated with coastal fronts are known to be important sources of instabilities. By smaller scale, we mean intermediate length scales lying between the Rossby deformation scale and the Rhines scale where the underlying dynamics are geostrophic to leading order and the β -effect remains an important non-negligible effect but does not enter into the dynamics at leading order. These models are referred to as *weak- β models* (Benilov 1992). The principal purpose of the present paper is to examine the nonlinear dynamics of these flows. It has been shown that the weak- β models, unlike their strong- β counterparts, exhibit linear baroclinic instability (Benilov 1992; Benilov & Cushman-Roisin 1994; Reszka & Swaters 1999a). As we shall show, the finite-amplitude effects can either accelerate the instability leading to explosive growth or, depending on the underlying parameters, inhibit the instability eventually saturating it. Our theoretical finite-amplitude analysis and numerical simulations suggest that the formation of coherent vortex structures during the destabilization of weak- β fronts is correlated with the presence of explosively unstable modal amplitudes.

The intermediate scale is of significant size in the ocean (Charney & Flierl 1981) and there is growing evidence of the increasing number and importance of oceanic phenomena that populate this scale (see Cushman-Roisin *et al.* 1992; Tang & Cushman-Roisin 1992; Benilov & Reznik 1996; Reszka & Swaters 1999a; and Part 1). These include unstable coastal fronts (Ikeda *et al.* 1984; McCreary, Fukamachi & Kundu 1991; Barth 1989a) and mesoscale ocean eddies (Olson *et al.* 1985). Recent analysis of TOPEX/POSEIDON data indicates that eddy energy in the ocean is concentrated at scales several times the deformation radius (Stammer 1997). As well, analysis of baroclinic waves often indicates a most unstable wavelength greater than the deformation scale (Griffith & Linden 1981; Griffiths *et al.* 1982; Ikeda & Emery 1984; Ikeda *et al.* 1984; and Flierl, Malanotte-Rizzoli & Zabusky 1987). In some cases, frontal instability was only observed when frontal widths exceeded several deformation radii (Griffiths & Linden 1981) and this is supported by primitive equation analysis (Killworth & Stern 1982). Increasing the motion amplitude (Griffiths *et al.* 1982) and nonlinear interactions (Ikeda & Emery 1984; Ikeda *et al.* 1984; McCreary *et al.* 1991) generally lead to yet larger scales.

Understanding the characteristics of these intermediate-scale phenomena has become increasingly important. Fronts contain large sources of available potential energy since the isopycnal configurations tend to be far from a state of no motion. This energy can be released if the front becomes unstable and small variations in the front grow to form large meanders and eddies. Such meanders and eddies are the main source of the mesoscale mixing and transport that occurs in the oceans. The proper resolution and/or inclusion of this eddy transport and mixing into ocean circulation models is an active area of research (see, for example, Barth 1989a; Bush *et al.* 1995; Greatbatch 1998; and Visbeck *et al.* 1997). On a smaller scale, unstable coastal currents play a significant role in the upwelling of nutrients and the creation of cross-shore flows (see Ikeda & Emery 1984; Ikeda *et al.* 1984; McCreary *et al.* 1991; Haidvogel, Beckman & Hedstrom 1991; and Barth 1989a). In all these examples of baroclinic instability, of greatest interest are finite-amplitude waves that have grown

to large meanders and eddies and are inherently nonlinear. Therefore, it is important to develop a comprehensive understanding of the nonlinear dynamics.

While analysis of nonlinear effects in QG models has provided great insight into aspects of nonlinear evolution of fronts, it also raises some questions. For QG models it was shown that nonlinear effects could suppress linear growth, leading to periodic amplitude modulation (Pedlosky 1987). A similar result holds for constant-PV models (Paldor 1987 and Ghil & Paldor 1994). Subsequently, nonlinear wave-wave interactions transfer energy to larger scales forming large meanders which then, through an interaction among various wavelengths, pinch off into eddies (Ikeda *et al.* 1984; Feliks & Ghil 1996). However, it was also concluded that extended QG theory would not properly describe the nonlinear dynamics because it does not discriminate between cyclones and anticyclones, while the latter are favoured in primitive-equation models and observations (Boss, Paldor & Thompson 1996). As well, these fronts have been shown to be unstable even when QG theory would have predicted stability (Paldor & Killworth 1987). In a turbulent ocean governed by QG dynamics, nonlinear interactions of eddies lead to a cascade of energy to the Rhines scale and the ultimate destination of any initial regime is decay into linear Rossby waves (Tang & Cushman-Roisin 1992). Yet, recent observations (Stammer 1997) indicate that the dominant eddy scale in the oceans is several times the deformation radius, significantly less than the Rhines scale. While it has been postulated that the forcing, topography or frictional effects can account for such a scale discrepancy, no unified theory exists. Together, these issues raise the question of whether the nonlinear, large-amplitude evolution of baroclinic instability can be properly modelled under the assumption of QG models.

On the other hand, the LAG models appear well suited to study these nonlinear effects. The LAG models retain not only the nonlinear advection of momentum but also the nonlinear mass transport inherent when large variations in frontal thickness are allowed. This fundamental nonlinear process of the primitive equations is not retained in the QG limit. The LAG models are similar in form to the layered QG model, and thus allow similar analysis while emphasizing the effects of large-amplitude isopycnal deflections. In contrast to the linear stability properties of the strong- β models (see Part 1), the weak- β models allow for vigorous baroclinic instability (except, of course, in the uncoupled model) in the form of large-scale baroclinic instability predicted by Griffiths & Linden (1981) and thus are appropriate to examine the nonlinear evolution of baroclinic instability.

In Reszka & Swaters (1999*a*), a finite-amplitude stability theory using the Swaters (1993*b*) model suggested that nonlinearities could both stabilize and further destabilize linearly unstable waves depending on the underlying parameter values. Most dramatically, numerical solutions illustrated the rapid development of eddies from both isolated and coupled fronts. These numerical solutions, and those of Reszka & Swaters (1999*b*), gave credibility to the belief that this relatively simple two-layer LAG model was capturing the essential physical process which led to the formation of cold and warm core eddies as well as jets and squirts similar to those seen in the numerical studies of McCreary *et al.* (1991), Haidvogel *et al.* (1991), Barth (1994) and Spall (1995), for example. In a study of geostrophic turbulence, LAG models have been shown to arrest the cascade of energy to larger scales, resulting in a concentration of energy at several times the deformation radius (Tang & Cushman-Roisin 1992). Thus, LAG models do capture observed features of oceanic fronts not modelled in the QG limit.

However, it has been argued that the nonlinear models examined previously are

not applicable to realistic ocean fronts as they impose too great a restriction on the depth of the front (Benilov & Reznik 1996). Within the weak- β models, the relative depth of the frontal layer, H_1 , to the total ocean depth, H , plays an important role in determining the exact mathematical form of the model. We can consider two limits for the depth ratio: the *thin-upper-layer* limit where $H_1 \ll H$ but where lower-layer motion is still important and the *equal-layers* limit where $H_1 \sim H$ and the motion in both layers contributes equally to the flow evolution. The *uncoupled* model, where the depth ratio becomes infinitesimal and the baroclinic flow evolves independent of the barotropic flow, is similar in form to the strong- β , uncoupled model but no longer retains any β -plane terms, see Part 1. In this paper, we examine the nonlinear aspects in the weak- β models for all depth ratios. In doing so, we illustrate the changes that occur as we extend the model to large depth ratios. As well, by presenting this analysis in conjunction with Part 1 which examines the nonlinear effects in strong- β models, we are able to present a complete analysis for all possible two-layer LAG models.

We also address the similarity of bottom topography and the β -effect within the weak- β LAG limit (see Karsten & Swaters 1999 for a complete discussion). On the intermediate scales of the weak- β models, often, e.g., for coastal currents, the background vorticity gradient supplied by bottom topography is more important than the β -effect. When bottom topography must be included in the dynamics, but is still a second-order effect, models analogous to the weak- β equations result (see the discussion in the Appendix or, for more details, Swaters 1991, 1993b and Karsten & Swaters 1999). While topography can play an essential role in the evolution of a front (see Reszka & Swaters 1999b), in this paper we will focus on weak- β models with no bottom topography. However, in the Appendix, we discuss how the models and analysis can be generalized to include the effects of bottom topography.

The plan of this paper is as follows. In §2, we give a brief derivation of the weak- β two-layer LAG models examined. In §3 and §4 we examine the equal-layers and thin-upper-layer models, respectively. In both sections, we begin by presenting the model equations, and a brief review of the linear stability characteristics and solutions is given. Next, based on the nonlinear invariants, we present a nonlinear stability analysis. Then, using the linear solutions, we present a finite-amplitude analysis that examines the evolution of a marginally unstable slowly varying wave-train under the influence of weak nonlinear effects. Because much of the work on the thin-upper-layer model has been presented previously, albeit in a different context, we will be brief in our presentation of this material. In §5, we describe numerical simulations of the weak- β LAG models concentrating on illustrating the finite-amplitude behaviour and the effects of varying the depth ratio. Finally, in §6, a summary and the conclusions of the paper as well as comments on future work are presented.

2. Model derivation

The weak- β two-layer large-amplitude geostrophic models are derived from the two-layer shallow-water equations following Benilov & Reznik (1996) (see also Cushman-Roisin *et al.* 1992 and Karsten & Swaters 1999). The underlying physical geometry is shown in figure 1 in Part 1. Under the assumptions of LAG dynamics, the two-layer shallow-water equations reduce to general LAG model, equation (2.1) and (2.2) in Part 1. The weak- β models are scaled such that the barotropic relative vorticity terms and β -plane term are of similar size, that is, when the length scale is the Rhines scale ($L = L_{LAGRh}$ and $\gamma = 1$ in the general equations in Part 1). The general LAG

equations reduce to

$$\Delta\psi_t + J(\psi, \Delta\psi) + \beta\psi_x + \mu\nabla \cdot [h(1 - \delta h)J(h, \nabla h)] = 0, \quad (2.1)$$

$$h_t + J(\psi, h) - \nu\nabla \cdot [h(1 - \delta h)(1 - 2\delta h)J(h, \nabla h)] = 0, \quad (2.2)$$

where h is the upper-layer depth and the leading-order baroclinic stream function and ψ is the barotropic stream function. These are *the general weak- β LAG equations*. The non-dimensional parameters are given by

$$\varepsilon = \frac{U}{f_0 L} = \left(\frac{R_I}{L}\right)^2, \quad \delta\mu = \frac{H_1}{H}, \quad \nu = \frac{\varepsilon}{\sqrt{\delta}}. \quad (2.3)$$

The parameter ε is the Rossby number defined in terms of the baroclinic velocity scale U , the Coriolis parameter f_0 and the horizontal length scale L , which reduces to the square of the ratio of the internal Rossby deformation ($R_I = \sqrt{g'H_1}/f$) to the length scale (see Part 1 for more details). As such, the weak- β model is truly an intermediate-scale model with $R_I \ll L \lesssim L_{LAGRh}$. (Note that if the length scale is less than the Rhines scale, the β -effect may not enter into the leading-order barotropic equation (2.1).) The depth ratio is split into two parts. The parameter δ measures the scale of the ratio; its choice determines the model. The parameter μ is an $O(1)$ parameter that allows variance of the depth ratio within the chosen model. The parameter ν compares the strength of the nonlinear frontal terms to the strength of the coupling term in the baroclinic equation. The auxiliary $O(1)$ parameter β is introduced to clearly indicate variance of β -effect after the scaling has been chosen.

Note that when the upper layer vanishes, $h = 0$, the model reduces to the equation

$$\Delta\psi_t + J(\psi, \Delta\psi) + \beta\psi_x = 0.$$

This equation describes the QG motion of a single layer on a β -plane in terms of the stream function ψ . This should be contrasted to the strong- β model where the equations do not describe *any* dynamics in this limit (see the discussion in Part 1).

For the analysis presented in this paper, we examine the fronts in a zonally periodic channel given by

$$\Omega = \{(x, y) \mid x_L < x < x_R, -\infty \leq W_1 < y < W_2 \leq \infty\}.$$

The periodicity represents the extended length scale in the east–west direction. All variables are assumed periodic in x . The boundary conditions simply reduce to the no-normal-flow conditions on the channel walls, that is, $h_x = \psi_x = 0$ on $y = W_{1,2}$. When fronts outcrop, additional boundary conditions are required at the outcropping (see Swaters 1993*b* and Karsten 1998). However, the appropriate *dynamic* boundary condition on an outcropping is the upper-layer PV equation itself when evaluated on the outcropping. And since the baroclinic equation is trivially satisfied when $h = 0$, it applies equally well on either side of the outcropping. This greatly simplifies the numerical modelling of outcropping fronts as no additional term that tracks the outcropping is required.

It is often useful to examine fronts which overlie bottom topography. As with QG models, the background vorticity gradient provided by bottom topography is similar to the β -plane effect. Bottom topography often becomes more important than the β -plane effect when coastal fronts are considered. Karsten & Swaters (1999) discuss the details of deriving LAG models when bottom topography is included. Here we note simply that the weak- β model can include the effects of bottom topography. In the Appendix, we present the model equations and how the analysis changes when

bottom topography is included. The domains and boundary conditions mentioned above can be used for coastal fronts if we define x as the along-front or shore coordinate and y as the cross-front or slope coordinate.

Finally, it should be noted that the geometric distortion associated with the approximation of the spherical Earth's surface with planar geometry can also be considered in the derivation of the LAG models. In Karsten & Swaters (1999), it was shown that this distortion leads to an additional term in the governing equations at high latitudes.

3. Equal-layers model

3.1. Model equations

The equal-layers model corresponds to a situation where the depth ratio is $O(1)$ and so we set

$$\delta = 1 \quad \text{and} \quad \nu = \varepsilon. \quad (3.1)$$

The model equations (2.1) and (2.2) reduce to

$$\Delta\psi_t + J(\psi, \Delta\psi + \beta y) + \mu J[h, h(1 - \mu h)\Delta h + \frac{1}{2}(1 - 2\mu h)|\nabla h|^2] = 0, \quad (3.2)$$

$$h_t + J(\psi, h) = 0, \quad (3.3)$$

where we have expanded the divergence terms using the Jacobian notation. These are the *weak- β equal-layers LAG equations*.

This model was first examined in Benilov (1992) and a reduced limit of this model, corresponding to $\mu h \ll 1$, was analysed in Benilov & Cushman-Roisin (1994). Due to the large upper-layer depth, (3.2) contains quartic nonlinearities in h . The strong coupling between the baroclinic and barotropic modes (the two are scaled equally) and the weak β -plane result in the baroclinic equation only balancing the diagnostic and coupling term.

The equal-layers model can be simplified through a transformation of variables presented in Benilov (1992). The transformation changes the frontal height $h(x, y, t)$ to a new variable $\bar{h}(x, y, t)$ defined by

$$\bar{h}(x, y, t) = \int_0^{h(x, y, t)} \sqrt{\mu\zeta(1 - \mu\zeta)} \, d\zeta. \quad (3.4)$$

It is not straightforward to give a physical interpretation for \bar{h} although it does appear to be some sort of a geometric average of the scaled layer depths μh and $1 - \mu h$.

Substituting (3.4) into (3.2) and (3.3) gives the transformed model equations

$$\Delta\psi_t + J(\psi, \Delta\psi + \beta y) + \mu J(\bar{h}, \Delta\bar{h}) = 0, \quad (3.5)$$

$$\bar{h}_t + J(\psi, \bar{h}) = 0. \quad (3.6)$$

This model is identical to the transformed model discussed in Benilov & Cushman-Roisin (1994), where the transformation (3.4) in the limit $\mu h \ll 1$ was used.

Under the transformation (3.4) certain regularity conditions must be imposed on the frontal height \bar{h} at an outcropping if \bar{h} is to be well defined there. Rather than discuss these conditions in detail, we will only use the transformed model to discuss fronts that do not outcrop. This suits the purpose of the nonlinear analysis that is the focus of this paper. For a complete discussion see Karsten (1998).

While the transformation (3.4) simplifies some of the analysis that follows, it obscures the physical insight somewhat since the connection between the quantity \bar{h}

and physical quantities such as the baroclinic velocity and PV is unclear. The fact that the transformation is not readily invertible is another drawback. As well, the use of a nonlinear transformation to study linear and weakly nonlinear aspects of a model is somewhat confusing. Yet, the transformation allows us to examine solutions that do not have restrictions on the initial amplitude of the basic state flow. This is a desirable attribute as it allows us to examine the extension of the analysis of gently-sloping fronts to the strong flows that the LAG models were originally designed to describe.

As in Part 1, we examine basic states that correspond to zonal flows where the frontal height varies only in the meridional direction. (Unlike Part 1, we will not assume that the barotropic flow is necessarily quiescent.) While some of the analysis is applicable, in principle, to fronts with outcroppings, the nonlinear analysis which is the focus of this paper assumes that fronts do not outcrop. Therefore, in the analysis of here and in §4, we assume that the basic-state upper-layer thickness does not outcrop.

3.2. Linear analysis

We briefly review some of the previous linear analyses and present linear solutions to the equal-layers model. In order to continue our analysis, we introduce the normal mode decomposition

$$\left. \begin{aligned} h(x, y, t) &= h_0(y) + \tilde{h}(y) \exp [i(kx - \omega t)] + \text{c.c.}, \\ \psi(x, y, t) &= \psi_0(y) + \tilde{\psi}(y) \exp [i(kx - \omega t)] + \text{c.c.}, \end{aligned} \right\} \quad (3.7)$$

where (h_0, ψ_0) are the mean flow and $(\tilde{h}, \tilde{\psi})$ are the amplitudes of a perturbation wave, $k \geq 0$ is the along-front wavenumber, $\omega = \omega_R + i\omega_I$ is the complex-valued frequency, and c.c. means complex conjugate. The phase and group velocities of the travelling wave are given by

$$c = c_R + ic_I = \frac{\omega}{k} \quad \text{and} \quad c_G = \frac{\partial \omega}{\partial k},$$

respectively. For the models examined in this paper, if the imaginary part of the frequency is non-zero, i.e. $\omega_I \neq 0$, then the front is linearly unstable and there exists a normal mode with an amplitude that will grow exponentially rapidly in time with a growth rate of $\sigma = |\omega_I| = k|c_I|$. If $\omega_I = 0$ the wave is neutrally stable.

The normal mode equations are found by substituting (3.7) into (3.2) and (3.3) and retaining only the linear perturbation terms giving

$$\begin{aligned} (c + \psi'_0)\tilde{\psi}'' - [(c + \psi'_0)k^2 + \psi_0''' + \beta]\tilde{\psi} \\ + \mu\{[h_0(1 - \mu h_0)(h'_0\tilde{h}' - h''_0\tilde{h})]' - h_0(1 - \mu h_0)h'_0k^2\tilde{h}\} = 0, \end{aligned} \quad (3.8)$$

$$[c + \psi'_0]\tilde{h} - h'_0\tilde{\psi} = 0. \quad (3.9)$$

The no-normal-flow conditions on the channel walls reduce to $\tilde{h}, \tilde{\psi} = 0$ on $y = W_{1,2}$. Linear boundary conditions at outcroppings can be derived as in Swaters (1993b), but are not needed here.

In terms of the variable \bar{h} , if we introduce

$$\bar{h}(x, y, t) = \bar{h}_0(y) + \tilde{\bar{h}}(y) \exp [i(kx - \omega t)] + \text{c.c.}, \quad (3.10)$$

it follows from (3.5) and (3.6) that normal mode equations are

$$(c + \psi'_0)\tilde{\psi}'' - [(c + \psi'_0)k^2 + \psi_0''' + \beta]\tilde{\psi} + [\bar{h}'_0\tilde{h}'' - (\bar{h}_0''' + k^2\bar{h}'_0)\tilde{h}] = 0, \quad (3.11)$$

$$[c + \psi'_0]\tilde{h} - \bar{h}'_0\tilde{\psi} = 0, \quad (3.12)$$

with $\tilde{h} = 0$ on $y = W_{1,2}$.

Analysis of these equations is given in Benilov (1992) and in Benilov & Cushman-Roisin (1994) for the reduced model. In particular, it was shown that monotonic, non-outcropping fronts are linearly stable as $k \rightarrow \infty$ only if

$$h'_0 = 0, \quad \forall W_1 \leq y \leq W_2.$$

Therefore only fronts of constant height are linearly stable for all wavenumbers. All other monotonic, non-outcropping fronts can be shown to be unstable as $k \rightarrow \infty$, that is, as the wavelength of the perturbations becomes very small. This result can be extended to outcropping fronts as well with a proper discussion of boundary conditions (see Karsten 1998). Since the shear associated with non-monotonic fronts is expected to destabilize fronts (see the discussion in Part 1 and Karsten 1998), and non-zonal flows are unstable (Benilov 1992), we expect that all fronts are unstable as length scales become small. Note that as $k \rightarrow \infty$ the assumption that all terms in (3.5) and (3.6) are $O(1)$ is invalid; the length scales have become too small to be modelled with the assumed underlying scaling. This problem of a model being unstable at small scales, beyond the scope of the model, will be discussed in more detail in the context of a linear solution below.

In the equal-layers model, the leading-order PV in each layer has gradients of opposite sign at all points except when $h'_0 = 0$. Thus, all flows satisfy the condition that instability in a two-layer QG model is possible if the PV gradient reverses sign across the layer interface (Pedlosky 1987). Assuming instability occurs, it is possible to derive restrictions on the values of c_R and c_I analogous to Howard's semi-circle theorem (Drazin & Reid 1981). But as the focus of this paper is nonlinear aspects, we leave this analysis for another time.

To complete the linear analysis and allow finite-amplitude analysis, we need to discuss solutions to the linear model. We present linear solutions for a gently sloping front and a wedge front of large amplitude. The analysis below does hold for a constant barotropic flow, $\psi'_0 = -U_0$, but as can be seen from (3.11) and (3.12) the effect of such a flow is only to vary the phase velocity by the value $-U_0$. As such, we choose $U_0 \equiv 0$ for the analysis of these fronts.

For a gently sloping front we take

$$h_0(y) = 1 + \alpha \left(y - \frac{W_2 - W_1}{2} \right), \quad W_1 \leq y \leq W_2, \quad (3.13)$$

where $h_0 > 0$ and $1 - \mu h_0 > 0$ for all y , that is, the thickness of either layer does not vanish. We also assume that the slope of the front, α , is small, that is

$$\alpha = \Delta \tilde{\alpha}, \quad (3.14)$$

where $0 < \Delta \ll 1$ and $\tilde{\alpha} = O(1)$. In order that non-trivial dynamics occurs (see (3.8) and (3.9)) we must also assume

$$\beta = \Delta \tilde{\beta}, \quad \omega = \Delta \tilde{\omega}, \quad c = \Delta \tilde{c}, \quad (3.15)$$

where $\tilde{\beta}$, $\tilde{\omega}$ and \tilde{c} are $O(1)$ parameters. (The rescaling of the frequency and phase

velocity is equivalent to rescaling time to a longer scale.) These rescalings allow us to examine what is essentially a QG flow, small-amplitude deflections in the interface, but at the longer time and large length scales of the LAG model.

Making the above substitutions into (3.8) and (3.9) gives, to leading order in Δ ,

$$\left. \begin{aligned} \tilde{c}\tilde{\psi}'' - [\tilde{c}k^2 + \tilde{\beta}]\tilde{\psi} + \mu(1-\mu)\tilde{\alpha}[\tilde{h}'' - k^2\tilde{h}] &= 0, \\ \tilde{c}\tilde{h} - \tilde{\alpha}\tilde{\psi} &= 0. \end{aligned} \right\} \quad (3.16)$$

In order to satisfy the boundary conditions, it follows that

$$\tilde{h} = A \sin(\ell y), \quad \ell = \frac{n\pi}{W_2 - W_1}, \quad n = 1, 2, 3, \dots, \quad (3.17)$$

where A is a free amplitude constant, with the dispersion relation

$$\tilde{c}(k, \ell) = \frac{-\tilde{\beta} \pm \sqrt{\tilde{\beta}^2 - 4\mu(1-\mu)\tilde{\alpha}^2 K^4}}{2K^2}, \quad (3.18)$$

where $K = \sqrt{k^2 + \ell^2}$ is the total wavenumber. The barotropic stream function is given by

$$\tilde{\psi} = \frac{\tilde{c}}{\tilde{\alpha}} \tilde{h}. \quad (3.19)$$

These solutions are unstable when the imaginary part of \tilde{c} is non-zero, that is, when the frontal slope exceeds a critical value

$$|\alpha| > \alpha_c = \frac{\tilde{\beta}}{2[\mu(1-\mu)]^{1/2} K^2}, \quad (3.20)$$

or, alternatively, if the length scale of the wave is sufficiently small so that the total wavenumber satisfies

$$K^4 > \frac{\tilde{\beta}^2}{4\mu(1-\mu)\tilde{\alpha}^2}. \quad (3.21)$$

This implies that all fronts will become unstable as k and ℓ become large, that is, as the wavelength of the motion becomes small. When the wave is unstable its growth rate $\tilde{\sigma}$ is given by

$$\tilde{\sigma} = k\tilde{c}_I = k \frac{\sqrt{-\tilde{\beta}^2 + 4\mu(1-\mu)\tilde{\alpha}^2 K^4}}{2K^2},$$

which grows linearly with k for large k . The group velocity for this solution is

$$\tilde{c}_G(k, \ell) = \frac{\tilde{\beta}\tilde{c}(k^2 - \ell^2) - 2\mu(1-\mu)\tilde{\alpha}^2 K^4}{2\tilde{c}K^2 + \tilde{\beta}}. \quad (3.22)$$

The expressions for the growth rate and conditions for instability allow a complete discussion of the small-scale instability. Fronts not only become unstable as the wavelength of the perturbation becomes small but, since the growth rate grows with k , the small-wavelength instabilities grow faster as their size decreases. Thus, the linear analysis leads to the conclusion that there will be catastrophic unstable growth at small (ultraviolet) wavelengths and hence is referred to as an ultraviolet catastrophe. The occurrence of an ultraviolet catastrophe in multi-layer strongly-coupled planetary geostrophic models is common (de Verdière 1986). This form of instability was also observed in the analysis of Paldor & Ghil (1990, 1991) and Barth (1994). Paldor & Ghil (1990) suggested that it is the availability of baroclinic energy

as seen through Reynolds stresses or phase differences between the two layers that leads to this vigorous short-wave instability when layer depths are of the same order. The difficulty with such instability is that the model is not self-contained, that is, the solution is driven outside of the region where the model applies (Benilov & Reznik 1996).

The form of the equations is critical for the possibility of an ultraviolet catastrophe. The balance of the QG-like terms and LAG terms in the barotropic equation (3.2) allows both to grow to large size. The absence of frontal terms in (3.3) means there are no terms preventing growth at small scales (compare this result to the linear result of §4.2 for the thin-upper-layer model where frontal terms are included in the baroclinic equation). The balance is not able to suppress this growth in the linear model. Whether or not nonlinear effects can suppress this growth is the focus of §3.4 and §5.1. As well, we examine whether the inclusion of higher-order Rossby number terms, especially the frontal terms, can suppress this growth.

Benilov & Cushman-Roisin (1994) found an exact solution to the transformed model linear stability equations (3.11) and (3.12) when \bar{h}_0 is given by the wedge front (3.13) with α is no longer assumed to be small. It is important to appreciate that this does not correspond to a linearly sloping front since the transformation (3.4) is nonlinear. Hereafter, this front will be referred to as the ‘wedge front’ to differentiate it from the ‘gently sloping front’ analysed above.

In this case the linear normal mode equations (3.11) and (3.12) reduce to

$$-c[\tilde{\psi}'' - k^2\tilde{\psi}] + \beta\tilde{\psi} - \alpha(\tilde{h}'' - k^2\tilde{h}) = 0,$$

$$c\tilde{h} - \alpha\tilde{\psi} = 0.$$

This equation is identical to (3.16) if $\mu(1 - \mu)$ is set to 1 and the tildes are dropped from α, β and c . Therefore, the solution (3.17)–(3.19) and formulas (3.20)–(3.22) hold appropriately. The similarity of the two solutions indicates that the solution for the gently sloping front is capturing the essential characteristics of the model despite assuming a relatively weak flow.

3.3. Nonlinear invariants and stability implications

We now discuss the invariants of the equal-layers model and use these to discuss nonlinear stability. In the definitions below we allow for the case of outcropping fronts. To do so, we introduce the domain \mathcal{F} as the subset of Ω where the upper layer exists, i.e. where $h \neq 0$, and the domain $\mathcal{N}\mathcal{F}$ as the subset where it does not, i.e. where $h = 0$.

The invariants can be derived by considering various conserved quantities of the shallow-water equations. Benilov (1992) showed that the functional given by

$$\mathcal{E}(h, \psi) = \frac{1}{2} \iint_{\Omega} |\nabla\psi|^2 dx dy - \frac{\mu}{2} \iint_{\mathcal{F}} h(1 - \mu h) |\nabla h|^2 dx dy \quad (3.23)$$

is an invariant of (3.2) and (3.3). Since \mathcal{E} corresponds to the difference between the barotropic kinetic energy (KE) and the baroclinic KE we refer to (3.23) as the pseudo-energy. The invariance of \mathcal{E} has important consequences for instability since it requires that both the barotropic and baroclinic modes must increase/decrease their KE concurrently (see §5).

There is also an invariant associated with the conservation of PV given by

$$\mathfrak{C}(h, \psi) = \iint_{\mathcal{N}\mathcal{F}} \Phi_2(\Delta\psi + \beta y) dx dy + \iint_{\mathcal{F}} (\Delta\psi + \beta y)\Phi_1(h) + \Phi_3(h) dx dy, \quad (3.24)$$

where Φ_1 , Φ_2 , and Φ_3 are sufficiently smooth functions of their arguments chosen so that any values associated with the variation of the outcropping are eliminated.

And, finally, we have the zonal momentum invariant given by

$$\mathfrak{M}(h, \psi) = \iint_{\Omega} y \Delta \psi \, dx \, dy. \quad (3.25)$$

Proving that these functionals are, in fact, conserved by the model can be done by using the governing equations and the boundary conditions or as a result of the conservation of energy and PV by the shallow-water equations (see Karsten 1998).

We can attempt to derive nonlinear stability conditions as in Karsten & Swaters (1996*b*). To do so we form the invariant functional

$$\mathfrak{I}(h, \psi) = \mathfrak{M}(h, \psi) - \mathfrak{M}(h_0, \psi_0) + \mathfrak{C}(h, \psi) - \mathfrak{C}(h_0, \psi_0), \quad (3.26)$$

where $(h_0, \psi_0) = (h_0(y), \psi_0(y))$ represents a basic-state zonal flow and \mathfrak{M} and \mathfrak{C} are given by (3.25) and (3.24), respectively, with the domains of integration extended to the entire domain Ω . (The first term in (3.24) vanishes since $\mathcal{N}\mathcal{F}$ vanishes when the upper layer is extended to the entire domain.) Then, from (3.26), we have

$$\mathfrak{I} = \iint_{\Omega} [y + \Phi_1(h)](\Delta \psi + \beta y) - [y + \Phi_1(h_0)](\Delta \psi_0 + \beta y) + \Phi_3(h) - \Phi_3(h_0) \, dx \, dy. \quad (3.27)$$

The first variation of \mathfrak{I} is given by

$$\delta \mathfrak{I} = \iint_{\Omega} \{ [\Phi_1'(h)(\Delta \psi + \beta y) + \Phi_3'(h)] \delta h + [y + \Phi_1(h)] \Delta \delta \psi \} \, dx \, dy.$$

In order that $\delta \mathfrak{I}$ vanishes for $(\psi, h) = (\psi_0, h_0)$, we choose Φ_1 and Φ_3 to satisfy

$$\Phi_1(h_0) = -y, \quad (3.28)$$

$$\Phi_3'(h_0) = -(\Delta \psi_0 + \beta y) \Phi_1'(h_0). \quad (3.29)$$

If we let $(h, \psi) = (h_0, \psi_0) + (\tilde{h}, \tilde{\psi})$, where $(\tilde{h}, \tilde{\psi})$ is a finite-amplitude perturbation, it follows from (3.27) using (3.28), that

$$\begin{aligned} \mathfrak{I}(\tilde{h} + h_0, \tilde{\psi} + \psi_0) &= \iint_{\Omega} \{ \Phi_3(h_0 + \tilde{h}) - \Phi_3(h_0) \\ &\quad + [\Phi_1(h_0 + \tilde{h}) - \Phi_1(h_0)] [\Delta(\psi_0 + \tilde{\psi}) + \beta y] \} \, dx \, dy. \end{aligned} \quad (3.30)$$

We assume that Φ_1 and Φ_3 satisfy the bounds

$$A_1 < \Phi_1'(\xi)(\Delta \psi_0 + \beta y) + \Phi_3'(\xi) < B_1, \quad \forall \xi > 0 \quad \text{and} \quad \forall y \in \Omega, \quad (3.31)$$

$$A_2 < \Phi_1'(\xi) < B_2, \quad \forall \xi > 0, \quad (3.32)$$

for some constants $A_{1,2}$ and $B_{1,2}$. If (3.31) is integrated twice, first from h_0 to ξ , using (3.29), and then from h_0 to $\tilde{h} + h_0$, and (3.32) is integrated once from h_0 to $\tilde{h} + h_0$ and taking the absolute value, it follows that

$$\frac{A_1}{2} \tilde{h}^2 < [\Phi_1(\tilde{h} + h_0) - \Phi_1(h_0)] [\Delta \psi_0 + \beta y] + \Phi_3(\tilde{h} + h_0) - \Phi_3(h_0) < \frac{B_1}{2} \tilde{h}^2, \quad (3.33)$$

$$|\Phi_1(\tilde{h} + h_0) - \Phi_1(h_0)| < \max(A_2, B_2) |\tilde{h}|. \quad (3.34)$$

Using (3.33) and (3.34) with (3.30) gives

$$\begin{aligned} \iint_{\Omega} \frac{A_1}{2} \tilde{h}^2 - \max(A_1, B_2) |\tilde{h}| |\Delta \tilde{\psi}| \, dx \, dy &< \mathfrak{J}(\tilde{h} + h_0, \tilde{\psi} + \psi_0) \\ &< \iint_{\Omega} \frac{B_1}{2} \tilde{h}^2 + \max(A_2, B_2) |\tilde{h}| |\Delta \tilde{\psi}| \, dx \, dy. \end{aligned} \quad (3.35)$$

In order to establish conditions for nonlinear stability, we need to establish conditions that guarantee that \mathfrak{J} is either positive or negative definite. To establish such bounds would require that we establish conditions such that the bound on the left (right) in (3.35) is positive (negative) definite for all perturbations. Such conditions would require an inequality of the form

$$\frac{A_1}{2} |\tilde{h}| \geq \max(A_2, B_2) |\Delta \tilde{\psi}|,$$

or

$$\frac{B_1}{2} |\tilde{h}| \leq -\max(A_2, B_2) |\Delta \tilde{\psi}|,$$

respectively. These conditions, in turn, require that the perturbation to the barotropic relative vorticity be somehow bounded by the perturbation to the upper-layer height, that is

$$|\Delta \tilde{\psi}| \leq C |\tilde{h}|, \quad (3.36)$$

for some positive constant C . This is clearly not true for general perturbations and specifically not true as length scales become small.

We can relate (3.36) to the analysis in §3.2 by associating $\Delta \tilde{\psi}$ with $k^2 \tilde{\psi}$. Then for (3.36) to hold, we require

$$k^2 |\tilde{\psi}| \leq C |\tilde{h}|,$$

which will only hold as $k \rightarrow \infty$ if we do not allow perturbations to the stream function, $\tilde{\psi} = 0$, or the perturbations to the frontal layer become large, $\tilde{h} \rightarrow \infty$. The latter case corresponds to instability, that is, unbounded growth in the perturbations, and the former is a restriction that allows for no barotropic flow and, from (3.3), only steady baroclinic flow and thus is trivially stable. Thus, although we cannot prove that it is impossible it is to establish nonlinear stability conditions, it appears to be unlikely since it is not possible to bound the small-scale growth.

3.4. Finite-amplitude analysis

In this subsection, the effects of the nonlinear terms in the model are examined. We begin by deriving the envelope equation governing the finite time and space evolution of the amplitude of a given wave-train. The method follows that of Pedlosky (1970, 1987), and is similar to the analysis of Mooney & Swaters (1996) and Reszka & Swaters (1999a). As in any weakly nonlinear calculation the details of the calculation are quite lengthy. In this paper, our presentation will be brief with the remaining details given fully and completely in Karsten (1998).

The finite-amplitude analysis is performed on a marginally unstable front. That is, we choose

$$\alpha = \alpha_c + v \Delta^2, \quad (3.37)$$

where α_c is the critical slope for instability given by (3.20) and v is an $O(1)$ parameter that allows us to adjust the size of the linear growth rate. For the gently sloping front,

the size of Δ is determined by the small slope of the basic state. For the wedge front we are free to choose Δ as long as it remains small.

In order to facilitate a weakly nonlinear analysis, slow space and time variables are introduced. These allow the space and time scales associated with the nonlinear interaction of the fundamental mode to be examined. This is done by letting

$$T = \Delta \tilde{t}, \quad X = \Delta x, \quad \mathfrak{X} = \Delta^2 x, \quad (3.38)$$

where for the gently sloping front $\tilde{t} = \Delta t$ in accordance with the necessary rescaling discussed in §3.2, while $\tilde{t} = t$ for the wedge front.

The perturbations are small in amplitude compared to the basic-state solution, and are expanded in an appropriate power series in Δ , that is

$$(h, \psi) = (h_0, 0) + \Delta^m [\Delta(h, \psi)^{(0)} + \Delta^2(h, \psi)^{(1)} + \Delta^3(h, \psi)^{(2)} + \dots], \quad (3.39)$$

where $m = 1$ for the gently sloping front to reflect that the perturbations are smaller than the $O(\Delta)$ frontal variations while $m = 0$ for the wedge front. Because of the underlying asymptotic approximations used to derive the weak- β models, the meridional boundary conditions are simply those discussed for the linear problem at all orders of Δ . In addition, as it turns out, there is no higher-order mean flow generated (full details can be found in Karsten 1998) and thus it is not necessary to impose additional boundary conditions on the zonally averaged stream function in the upper and lower layers as one does in, for example, weakly nonlinear baroclinic instability in the Phillips model (see Pedlosky 1987).

Taking into consideration (3.38) and (3.39) the model equations (3.2) and (3.3) can be expanded in powers of Δ . Setting the coefficients of terms in similar orders of Δ to zero gives a series of problems that must be solved. The solvability conditions that arise at each order eventually give rise to an evolution equation for the slowly varying amplitude of the linear solution.

The leading-order problem is the linear stability problem for the given basic state as discussed in §3.2. The solution is given by

$$\left. \begin{aligned} h^{(0)} &= A(X, \mathfrak{X}, T) \tilde{h}(y) \exp [i(kx - \omega t)] + \text{c.c.}, \\ \psi^{(0)} &= A(X, \mathfrak{X}, T) \tilde{\psi}(y) \exp [i(kx - \omega t)] + \text{c.c.}, \end{aligned} \right\} \quad (3.40)$$

where $A(X, \mathfrak{X}, T)$ is the slowly varying amplitude. The functions \tilde{h} and $\tilde{\psi}$ are given by (3.17) and (3.19), respectively, with the frequency determined by (3.18).

At the next order, an asymptotically consistent solution can only be found provided

$$A_X = 0. \quad (3.41)$$

Similarly, all variables are henceforth assumed independent of X . The group velocity, given by (3.22) is infinite at $\alpha = \alpha_c$. Thus (3.41) is the simple statement that to this order the wave amplitude, and thus the wave energy, travels at the group velocity. Finally, in the third-order problem, an asymptotically consistent solution can only be found provided

$$A_{TT} + i\chi A_{\mathfrak{X}} = (\sigma^2 - \Gamma)A - N(|A|^2 - |A_0|^2)A, \quad (3.42)$$

where $A_0 = A(T = 0)$.

For the gently sloping front the coefficients in (3.42) are given by

$$\chi = \frac{k^3 \beta^2}{(k^2 + \ell^2)^3}, \quad (3.43)$$

$$\sigma^2 = \frac{vk^2\beta\mu(1-\mu)}{K^2}, \quad (3.44)$$

$$N = \frac{2\mu(1-\mu)k^2\ell^2(k^2-\ell^2)}{K^2}, \quad (3.45)$$

$$\Gamma = -\frac{2}{L(k^2+\ell^2)} \int_0^L \gamma(y)\tilde{h}(y) dy, \quad (3.46)$$

where the details of the derivation of the kernel function $\gamma(y)$ are discussed fully in Karsten (1998) but are not particularly important in the analysis presented here and thus omitted. For the wedge front, the coefficients are the same with $\mu(1-\mu)$ set to 1 and $\Gamma = 0$.

The fact that the evolution equations are almost identical for the two basic states is not surprising. However it should be stressed that the second analysis of this section holds for wedge fronts with no limitations on the frontal slope, while the gently sloping front analysis assumed the frontal slope was small. This leads to the very important conclusion that the weakly nonlinear analysis that is performed under the simplifying assumptions of a gently sloping front does indeed capture the essential nonlinear aspects of the model even when these assumptions break down. However, the similarity of the evolution equations is also a result of the similarity of the eigenfunctions and hence, the expansion of the nonlinear terms. As shown in the analysis of the strong- β model, if the structure of the eigenfunctions changes a greater array of interactions can occur (see Part 1). However, our analysis of the weak- β model indicates that the analysis of the gently sloping front does capture the qualitative behaviour of the nonlinear effects.

Before discussing solutions of (3.42), it should be noted that the assumption that $\alpha_c > 0$ is not important in the analysis. Indeed, the above analysis can be carried out with $\alpha_c < 0$ and the same evolution equation is obtained. The only change that occurs is that in this case

$$\alpha = \alpha_c - vA^2.$$

This is reasonable as the linear results are also identical for positive and negative α which, in turn, implies that these results are symmetric for eastward and westward flows.

We write equation (3.42) in a slightly simpler form by introducing

$$\zeta = \sigma^2 - \Gamma + N|A_0|^2, \quad (3.47)$$

giving

$$A_{TT} + i\chi A_x = \zeta A - NA|A|^2. \quad (3.48)$$

Equation (3.48) is the unstable nonlinear Schrödinger equation (UNLS) derived, in the geophysical fluid dynamics context, by Pedlosky (1972) and discussed further in Tan & Liu (1995) for the two-layer Phillips model and derived in Mooney & Swaters (1996) for the Swaters (1991) model in the context of bottom-intensified frontal dynamics on sloping topography.

Referring to (3.42), the parameter σ represents the small linear growth of the marginally unstable mode. The parameter N represents the result of the nonlinear interactions. The parameter Γ represents the corrections to the linear growth rate as higher-order linear terms are considered. The manner in which Γ depends on the y structure of the linear solution is discussed in Karsten (1998). For the wedge front, all fast-varying linear terms are included in the leading-order problem and no such

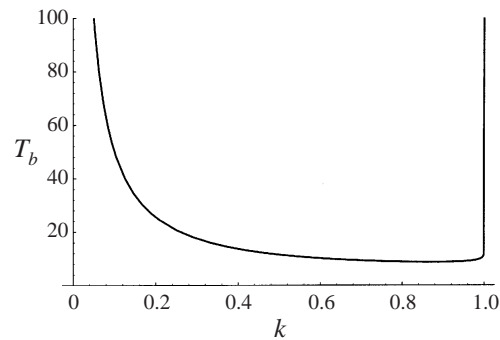


FIGURE 1. The blow-up time for solutions with $k < \ell$. The blow-up time becomes infinite as k tends to zero and ℓ is a minimum at $k \approx 0.8\ell$.

correction occurs, that is $\Gamma = 0$. These correction terms can either stabilize or further destabilize the front moving the marginal stability curve. In the following analysis, we wish only to consider the nonlinear modulation of a marginally unstable front and therefore assume that $\sigma^2 - \Gamma$ is positive. We do present some brief analysis of marginally stable fronts at the end of this section, and cases where $\sigma^2 - \Gamma$ is negative are included in this analysis.

Assuming linear instability, the question we wish to answer is how the nonlinearities affect the unstable growth. The nonlinear terms in the UNLS will dampen the growth of the instability when $N > 0$, and will enhance the growth of the instability when $N < 0$. The fact that N changes signs when $k = \ell$ in this model will lead to additional analysis not found in, for example, Pedlosky (1970) or Mooney & Swaters (1996) but similar to that found in Reszka & Swaters (1999a). On the other hand, the lack of a critical shear value, a positive critical value of $|\alpha|$ that must be exceeded for instability, results in no analysis analogous to the critical shear analysis found in Pedlosky (1982) and Mooney & Swaters (1996).

We can easily determine the effect of the nonlinear terms by examining solutions to (3.48) that are real and independent of \mathfrak{X} (see Pedlosky 1970 or Mooney & Swaters 1996). If $N > 0$ the solution is a bounded periodic solution. The exact form depends on ς , N and the initial conditions. One can provide a detailed analysis of the characteristics of these solutions but these aspects are not the focus of this work (see Reszka & Swaters 1999a; Karsten 1998; or Mooney & Swaters 1996). If we include spatial variability, it can be shown that the stable, periodic solutions found when $N > 0$ can be associated with travelling-wave and soliton solutions (see Karsten 1998). Thus, when the nonlinear effects are stabilizing, they act to reorganize the wave-train into travelling-wave solutions that have an oscillating amplitude or into soliton solutions of small but finite amplitude.

On the other hand, if nonlinear effects enhance the linear growth, that is, if $N < 0$, the solution becomes infinite in finite time, i.e. explosive instability. This occurs for all cases where the zonal wavelength of the perturbation exceeds the meridional wavelength, that is, when $k < \ell$. The solutions grow initially due to the linear instability and, as the amplitude becomes finite, nonlinear terms actually enhance the growth. The growth continues to accelerate leading to the amplitude becoming infinite in finite time.

This finite blow-up time can be calculated and is plotted in figure 1 versus the ratio k/ℓ for $\beta = 1$ and $\mu = 0.5$. The blow-up time becomes large as k tends to ℓ

and zero. The time of blow-up is a minimum at an along-channel wavenumber just slightly less than the cross-channel wavenumber, $k \approx 0.9\ell$, where $T_b = 8.4$. For a mid-latitude flow with a typical Rossby number of 0.1, this corresponds to roughly one day. Thus, a marginally unstable wave will grow rapidly to full nonlinearity if its zonal wavelength is greater than its meridional wavelength. This growth can occur at all scales indicating that the ultraviolet catastrophe resulting from the linear analysis will not be suppressed by nonlinear effects but only shifted to waves where the zonal wavelength exceeds the meridional wavelength. In fact, the size of N , and thus the growth rate, increases as the length scale decreases, indicating that the ultraviolet catastrophe will be enhanced. Therefore, it is expected that any initial front will be dominated by small-scale waves beyond the resolution of the model.

However, in § 5.3 we illustrate that if the nonlinear frontal terms are retained in the baroclinic equation, small-scale instabilities are suppressed. In this case we see rapid growth of large-scale waves with zonal wavelength slightly greater than meridional wavelength. As the wave amplitude becomes large, here illustrated by the blow-up of the amplitude, the wave will become fully nonlinear. In the fully nonlinear regime, it is expected that nonlinear effects will eventually suppress the unstable growth leading to stable, large-amplitude, large-scale structures (see § 5). This process differs from the previous descriptions of eddy formation via finite-amplitude analysis. In previous approaches, the nonlinear terms are shown to modulate the linear growth allowing the formation of wave-packet/soliton structures that are theorized to represent eddies. Here, however, the theory suggests that nonlinear effects can enhance the growth of an unstable wave. Thus, a single unstable wave can grow to large amplitude resulting in large meanders that may pinch off into eddies. This process is clearly illustrated in the numerical solutions of § 5.

It should be noted that the nonlinear effects as described by N do not change with β . Hence, varying the latitude of a flow (and the bottom topography as shown in the Appendix) does not change the effect of the nonlinearities. This is not to say that these have no effect, as the linear marginal stability curve and growth rate are directly affected by changes in β , with higher β stabilizing the flow as expected. But, the strength of the β -plane does not determine the scales at which the rapid nonlinear growth occurs. Hence, one might expect to see the final scales of waves/eddies resulting from baroclinic instability to be independent of the β -effect. This could help explain why the cascade of energy to the Rhines scale seen in QG analysis can be suppressed in the LAG formulation.

The above analysis leads to the question of how the nonlinear processes affect linearly stable flows. The above analysis can be repeated for a marginally stable flow equally well if we choose

$$\alpha = \alpha_c - v_s A^2, \quad (3.49)$$

as opposed to (3.37). The analysis is identical to that presented above and leads to (3.48) with $v = -v_s$. The only change is that the linear term in (3.48), which before was dominated by the contribution of the linearly unstable growth rate σ , corresponds to a linearly stable wave and is of the opposite sign. Thus, all solutions will be initially stable and their amplitudes will oscillate. If one examines solutions to (3.48) when $\varsigma < 0$ and $N > 0$, nonlinear terms act to destabilize the linearly stable flow. But, solutions which are unstable and become infinite in finite time are only possible if $A'_0 \equiv A_T(T = 0)$ takes a sufficiently large value (see Karsten 1998 for details). A physical choice for A'_0 would be setting it to zero to reflect the neutral growth of amplitude associated with a linearly stable solution. Giving A'_0 a large positive value

corresponds to giving the initial solution a large kick of energy allowing its amplitude to grow and may not be physical.

4. Thin-upper-layer model

In this section, we present an analysis of the thin-upper-layer model analogous to that presented in §3. Some of these results have been established before in Swaters (1993*b*), Karsten & Swaters (1996*b*) and Reszka & Swaters (1999*a*). Thus, our presentation here is brief.

4.1. Model equations

The thin-upper-layer model corresponds to a situation where the upper layer is much thinner than the lower layer and we set

$$\delta = \varepsilon^2 \quad \text{and} \quad \nu = 1.$$

The model equations (2.1) and (2.2) reduce to

$$\Delta\psi_t + J(\psi, \Delta\psi) + \beta\psi_x + \mu J(h, h\Delta h + \frac{1}{2}|\nabla h|^2) = 0, \quad (4.1)$$

$$h_t + J(\psi, h) - J(h, h\Delta h + \frac{1}{2}|\nabla h|^2) = 0. \quad (4.2)$$

These are the *weak- β thin-upper-layer LAG equations*. It should be noted that the length scale of this model is an intermediate scale lying between the deformation radii associated with the upper and lower layers (Reszka & Swaters 1999*a*). This restricts the flows which it can be applied to as this ‘intermediate region’ decreases in size as the depth ratio increases.

The cubic nonlinear terms can be eliminated from (4.1) by forming (4.1) + $\mu \times$ (4.2) to give

$$(\Delta\psi + \mu h)_t + J(\psi, \Delta\psi + \mu h + \beta y) = 0. \quad (4.3)$$

Due to the thinness of the upper layer the frontal terms are now only cubically nonlinear and the weak coupling allows the frontal term to enter the leading-order balance in the baroclinic equation.

4.2. Linear analysis

The linear stability analysis for the thin-upper-layer model was presented in Swaters (1993*b*), where it was established that the steady solution $(h_0(y), \psi_0(y))$ is linearly stable if

$$-(\psi_0''' + \beta) > \mu h_0' > 0, \quad \forall y,$$

or

$$-(\psi_0''' + \beta) < \mu h_0' < 0, \quad \forall y.$$

These conditions establish that the leading-order PV gradients in the two layers are everywhere of the same sign.

In Reszka & Swaters (1999*a*), the solution to the linear stability problem for the gently sloping front (3.13) was found with \tilde{h} given by (3.17), the phase velocity given by

$$\tilde{c}(k, \ell) = \frac{-\tilde{\beta} - \tilde{\alpha}K^4 \pm \sqrt{(\tilde{\beta} + \tilde{\alpha}K^4)^2 - 4\tilde{\alpha}(\mu\tilde{\alpha} + \tilde{\beta})K^4}}{2K^2}, \quad (4.4)$$

and the barotropic stream function given by

$$\tilde{\psi} = \left[K^2 + \frac{\tilde{c}}{\tilde{\alpha}} \right] \tilde{h}.$$

Eastward and westward flows no longer give identical results. The waves are unstable whenever

$$(\tilde{\beta} - \tilde{\alpha}K^4)^2 - 4\mu\tilde{\alpha}^2K^4 < 0,$$

which is not invariant under $\alpha \rightarrow -\alpha$. This gives rise to two marginal stability curves,

$$\tilde{\alpha}_{c_1} = \frac{\tilde{\beta}}{K^2(K^2 + 2\sqrt{\mu})}, \quad (4.5)$$

$$\tilde{\alpha}_{c_2} = \frac{\tilde{\beta}}{K^2(K^2 - 2\sqrt{\mu})}, \quad (4.6)$$

where the first curve corresponds to the lower branch and the second to the upper branch of the marginal stability boundary given in Reszka & Swaters (1999a).

The inclusion of the nonlinear Jacobian terms in the baroclinic equation establishes a high-wavenumber cutoff for instability. That is, instability occurs only for

$$\left. \begin{aligned} \frac{-\sqrt{\mu\tilde{\alpha}} + \sqrt{\mu\tilde{\alpha} + \tilde{\beta}}}{\sqrt{\tilde{\alpha}}} \leq K^2 \leq \frac{\sqrt{\mu\tilde{\alpha}} + \sqrt{\mu\tilde{\alpha} + \tilde{\beta}}}{\sqrt{\tilde{\alpha}}}, \\ \frac{\sqrt{-\mu\tilde{\alpha}} - \sqrt{-\mu\tilde{\alpha} + \tilde{\beta}}}{\sqrt{-\tilde{\alpha}}} \leq K^2 \leq \frac{\sqrt{-\mu\tilde{\alpha}} + \sqrt{-\mu\tilde{\alpha} + \tilde{\beta}}}{\sqrt{-\tilde{\alpha}}}, \end{aligned} \right\} \quad (4.7)$$

for $\tilde{\alpha} > 0$ and $\tilde{\alpha} < 0$, respectively. Thus, the ultraviolet catastrophe seen for the equal-layers model does not occur here. As μ becomes large, the high-wavenumber cutoffs given in (4.7) both become large. In this limit the results tend to that of the equal-layers model.

4.3. Nonlinear invariants and a stability theorem

The nonlinear invariants and aspects of the nonlinear stability theory were presented in Swaters (1993b) and Karsten & Swaters (1996b). Here, without derivation, we simply list the invariants. They are

$$\mathcal{E} = \frac{1}{2} \iint_{\Omega} |\nabla\psi|^2 \, dx \, dy - \frac{1}{2} \iint_{\mathcal{F}} h |\nabla h|^2 \, dx \, dy, \quad (4.8)$$

$$\mathcal{C} = \iint_{\Omega} \Phi_1(\Delta\psi + \mu h + \beta y) \, dx \, dy + \iint_{\mathcal{F}} \Phi_2(h) \, dx \, dy, \quad (4.9)$$

$$\mathfrak{M} = \iint_{\Omega} y \Delta\psi \, dx \, dy, \quad (4.10)$$

representing the Hamiltonian or pseudo-energy invariant, the Casimir associated with the leading-order PV for the lower and upper layers and the zonal momentum invariant, respectively.

Using (4.8) (see Swaters 1993b) or the zonal momentum invariant (4.10) (see Karsten & Swaters 1996b) it is possible to establish linear and nonlinear stability theorems. Here we present the conditions corresponding to those found using the

zonal momentum invariant as they correspond to the linear conditions presented above and are these easiest to interpret. The stability conditions are determined by considering the pseudo-momentum

$$\mathfrak{J}(\tilde{h} + h_0, \tilde{\psi} + \psi_0) = \mathfrak{M}(\tilde{h} + h_0, \tilde{\psi} + \psi_0) - \mathfrak{M}(h_0, \psi_0) + \mathfrak{C}(\tilde{h} + h_0, \tilde{\psi} + \psi_0) - \mathfrak{C}(h_0, \psi_0), \quad (4.11)$$

where $(h_0, \psi_0) = (h_0(y), \psi_0(y))$ represents a basic-state zonal flow, $(\tilde{h}, \tilde{\psi})$ is the perturbation to this flow, and \mathfrak{M} and \mathfrak{C} are given by (4.10) and (4.9), respectively, with the region of integration extended to the entire domain Ω . The following nonlinear stability result was established by Karsten & Swaters (1996b).

THEOREM 4.1. *The zonal flow $(h_0(y), \psi_0(y))$ is nonlinearly stable in the sense of Liapunov with respect to the perturbation norm*

$$\|(\tilde{h}, \tilde{\psi})\|^2 = \iint_{\Omega} (\Delta\tilde{\psi} + \tilde{h})^2 + \tilde{h}^2 \, dx \, dy,$$

if there exists real constants $A_{1,2}$ and $B_{1,2}$ such that either

$$0 < A_1 \leq \Phi_1''(\xi) \leq B_1 < \infty \quad \text{and} \quad 0 < A_2 \leq \Phi_2''(\xi) \leq B_2 < \infty, \quad (4.12)$$

or

$$-\infty < A_1 \leq \Phi_1''(\xi) \leq B_1 < 0 \quad \text{and} \quad -\infty < A_2 \leq \Phi_2''(\xi) \leq B_2 < 0 \quad (4.13)$$

for all $\xi \in \mathbb{R}$ where

$$\Phi_1'(\Delta\psi_0 + \mu h_0 + \beta y) = -y, \quad \Phi_2'(h_0) = y. \quad (4.14)$$

Equations (4.14) establish that the first variation of \mathfrak{J} vanishes when evaluated at $(h_0(y), \psi_0(y))$. Conditions (4.12) and (4.13) establish that \mathfrak{J} is either positive or negative definite, respectively, and Liapunov stability conditions follow accordingly.

The interpretation of these stability conditions is not trivial. Nonlinear stability can only be established if linear stability holds, that is, if the PV gradients are everywhere of the same sign. However, the nonlinear conditions are more strict than the linear conditions in that (4.12) and (4.13) must hold for all values of ξ and not only when evaluated for the basic state. As such, having the PV gradients everywhere of the same sign does not guarantee nonlinear stability (see Karsten & Swaters 1996b for more details and examples).

4.4. Finite-amplitude analysis

A weakly nonlinear analysis of the thin-upper-layer model analogous to that carried out in §3.4 is presented in detail in Reszka & Swaters (1999a). If one generalizes these results by including the parameters μ and β , the analysis results in an evolution equation identical to (3.48) where now

$$\chi = \frac{\mu k \beta^2 [(1 - \mu)(K^2 \pm \sqrt{\mu})^2 + 2(1 + \mu)k^2(K^2 \pm \sqrt{\mu})]}{K^4(K^2 \pm 2\sqrt{\mu})^2[\mu(1 - \mu) \pm \sqrt{\mu}K^2]}, \quad (4.15)$$

$$\sigma^2 = \frac{vk^2\beta\sqrt{\mu}}{K^2}, \quad (4.16)$$

$$N = \mu k^2 \ell^2 \left[1 + \frac{(K^2 - 4\ell^2)(K^2 \pm \sqrt{\mu})}{\mu(1 - \mu) \pm \sqrt{\mu}K^2} \right], \quad (4.17)$$

where the upper + sign corresponds to the marginal stability curve (4.5) and the lower – sign to (4.6). The term Γ has a very complicated form (see Reszka 1997). These results extend the results of Reszka & Swaters (1999a) where it was assumed that $\tilde{\beta} = -1$ and $\mu = 1$. It is clear that the nonlinear effects, the spatial variation, and the dependence on the parameter μ are much more complicated in the thin-upper-layer model than in the equal-layers model.

Solutions follow as in § 3.4 or Reszka & Swaters (1999a). There are again two basic forms of solutions: periodic modulation of the linearly unstable mode when $N > 0$ and explosive nonlinear instability when $N < 0$. The behaviour of the solutions differs for the two marginal stability curves. For the curve given by (4.5) and corresponding to the upper sign in (4.15)–(4.17) the analysis is very similar to that for the equal-layers model presented in § 3.4. As with the equal-layers model $N > 0$ when $k > k_c$ and $N < 0$ when $k < k_c$ where now

$$k_c^2 = \ell^2 - \sqrt{\mu} + \sqrt{4\ell^4 + \mu^2}. \quad (4.18)$$

Here, k_c is no longer simply ℓ but is generally larger than ℓ but less than $\sqrt{3}\ell$. Thus, the range of wavenumbers that lead to nonlinear growth has been increased.

For the marginal stability curve given by (4.6) and corresponding to the lower sign in (4.15)–(4.17) the story is different. Here, $N > 0$ when $k_{c-} < k < k_{c+}$ and $N < 0$ elsewhere with

$$k_{c\pm}^2 = \ell^2 + \sqrt{\mu} \pm \sqrt{4\ell^4 + \mu^2}. \quad (4.19)$$

Thus, the solutions grow nonlinearly for very large values of k and sometimes for small values of k (k_{c-}^2 becomes negative for many parameter values and hence no lower bound exists). Since the magnitude of N grows with k , and the nonlinear growth increases with N , for this marginal stability curve the nonlinear growth rate is largest for the smallest scale. This is a result akin to the ultraviolet catastrophe discussed in § 3.2. However, as discussed in Reszka (1997), the parameter values at which this growth occurs are not in line with the asymptotic approximations made for this solution. That is, for typical parameter values $\mu = \ell = 1$ and taking $k = k_{c+} = 2 + \sqrt{5}$, we have from (4.6) that $\alpha_{c-} \approx \beta/17$. But it was assumed $\tilde{\alpha}$ and $\tilde{\beta}$ were of similar size (see (3.13) and (3.14)). Thus, the analysis begins to break down while the linear growth rate becomes extremely small. It should be noted that for parameter values that give rise to $\alpha_{c-} < 0$, that is, the instability region given by the second equation in (4.7), the nonlinear terms modulate the linear growth.

We conclude that the nonlinear terms in the thin-upper-layer model act to create nonlinear growth for westward flows, $\alpha > 0$, and zonal scales which are on the order of or less than the meridional scales. At the small scales of the high-wavenumber cutoff the analysis begins to break down. For eastward flows, $\alpha < 0$, the nonlinear terms are generally stabilizing.

5. Numerical solutions

In this section, the weak- β models are solved using a straightforward numerical scheme. It is not our goal to provide an extensive investigation into all possible parameter values and frontal geometries. Rather, we identify what we believe to be the important aspects of the model, most notably how the analytical results of § 3 and § 4 manifest themselves in the fully nonlinear regime and how the nonlinear evolution changes as the depth ratio varies.

The algorithm we use is straightforward: an explicit, finite-difference scheme that

is leapfrog in time and central in space. The Jacobian terms are approximated using the Arakawa (1966) scheme. The simulations are run in a zonally periodic channel with no-normal-flow conditions at the channel walls. The algorithm is similar to that used in Reszka & Swaters (1999a). The baroclinic equation is simply stepped forward in time giving the frontal height. The barotropic equation is stepped forward in time giving the barotropic relative vorticity. The stream function is then found using a Laplacian inversion scheme. In the simulations, we employ two types of numerical friction as discussed in Part 1. The first eliminates negative values of the frontal height and the second is a high-power harmonic friction. Use of numerical friction does result in a small increase in mass and affects the conservation of the model invariants. As well, numerical friction dissipates the energy at very small scales.

5.1. *Equal-layers model*

For the equal-layers model discussed in §3, the theoretical analysis predicts linear instability and explosive nonlinear instability at small wavenumbers. For all numerical simulations run, small-scale waves grow and continue to form even smaller-scale structures until we have a turbulent current. No large-scale structures are seen and the results are independent of the form of the initial perturbation, the inclusion of friction, or the structure of the basic state. Obviously, the ultraviolet catastrophe predicted by the linear and nonlinear analysis is being observed. Once again, this illustrates that flows modelled by the equal-layers weak- β model are pushed to scales beyond the resolution of the model. However, as we illustrate in §5.3, if we include the nonlinear frontal terms in the baroclinic equation, this small-scale growth can be suppressed and large-scale features exhibiting characteristics consistent with the analysis of §3 are observed.

As the instability grows, there is a small release of mean potential energy (PE) allowing a small growth of the perturbation amplitude. As expected, there is a large growth in both the baroclinic KE and the barotropic KE as small scales begin to dominate the flow. The fact that the baroclinic and barotropic KE grow concurrently is required by the conservation of the pseudo-energy \mathcal{E} .

5.2. *Thin-upper-layer model*

A detailed examination of numerical simulations using the thin-upper-layer model is presented in Reszka & Swaters (1999a). Here, we briefly recap some of these results while examining a simulation that allows direct comparison to the discussion that follows. For isolated fronts, Reszka & Swaters (1999a) demonstrated that large-scale waves can grow to finite size, often pinching off into warm core eddies or enclosing cold core eddies. These large-scale waves can also be nonlinearly modulated with amplitudes that oscillate in time. The conditions that separate these two forms of solutions are not fully understood but there is no doubt that they are related to the two forms of nonlinear effects seen in the finite-amplitude analysis. The development of a barotropic Rossby wave in the lower layer is essential in the instability process. It is the coupling of this wave to the baroclinic dynamics that initiates the instability (Reszka & Swaters 1999a).

For our purpose we present an example simulation for an isolated front for comparison to the simulations run for the equal-layers model. The results are shown in figure 2. The figure shows the development of a large-scale wave and corresponding barotropic cells. In this rapidly developing instability, the meanders develop large filaments which pinch off to form eddies. These eddies are often reabsorbed by adjacent filaments. In slower developing instabilities, the cyclonic barotropic cells

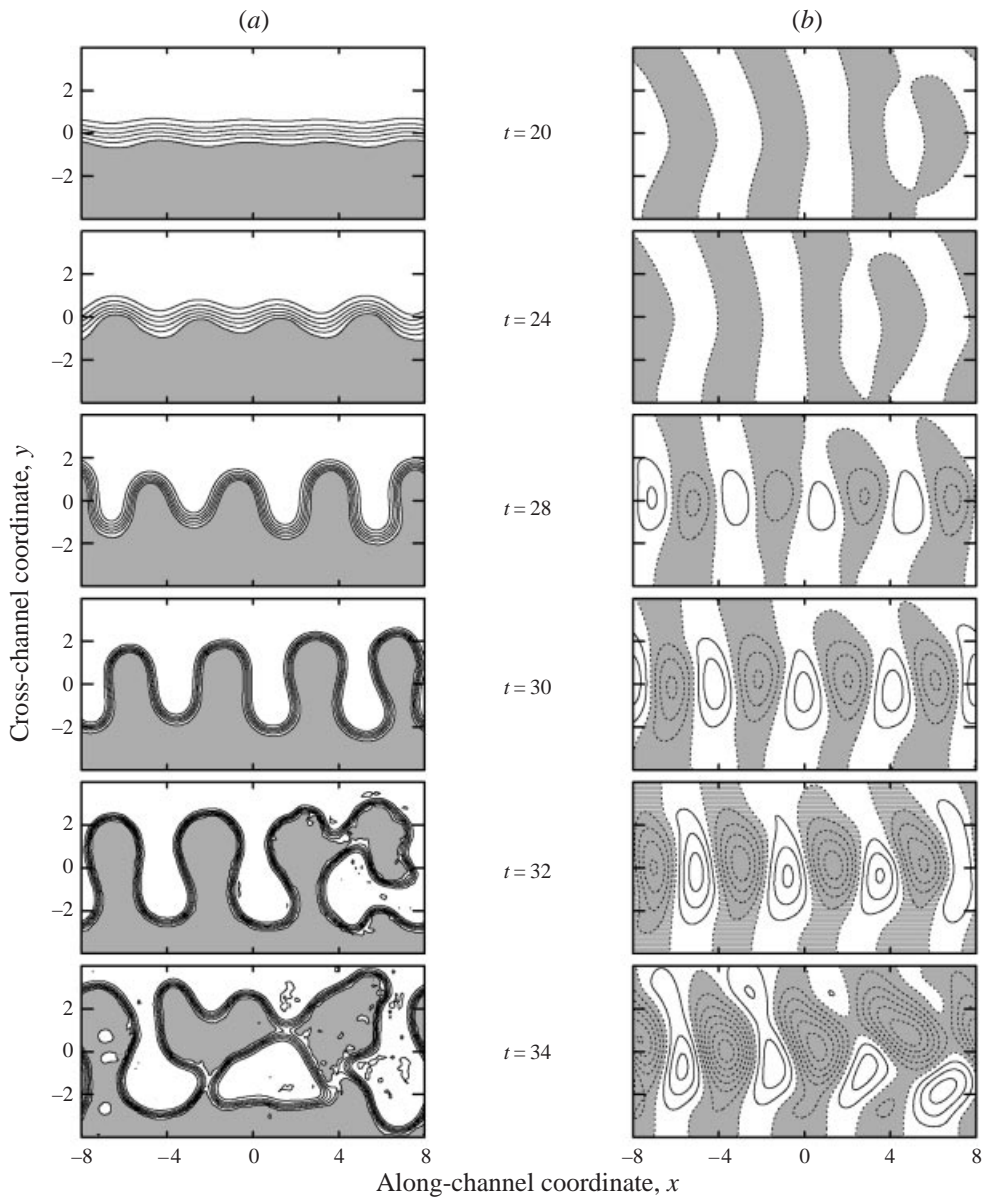


FIGURE 2. Results of the numerical simulation of the thin-upper-layer simulation: (a) The contours of the upper-layer height. The grey regions are where the upper layer vanishes; (b) and the contour increment is 0.1. The contours of the barotropic stream function. The grey regions are where the stream function is negative; and the contour increment is 0.04.

cause the waves to break backwards often enclosing cold-core eddies (see Reszka & Swaters 1999*a, b*). The zonal and meridional length scales of these meanders and eddies are always similar. As the instability grows, the current is concentrated, resulting in high gradients and corresponding velocities. In terms of energy, there is an initial release of mean KE as the large wave begins to grow. This initiates a release of available PE and the instability grows rapidly with large increases in baroclinic and barotropic KE. Again, this behaviour is predicted by the pseudo-energy \mathcal{E} as it

requires equivalent growth in baroclinic and barotropic KE. The PE is only released when large-scale structures, which rapidly flatten out the mean front profile, have formed.

In Reszka & Swaters (1999*a, b*) the thin-upper-layer model was used to examine a current similar to the California Current System and the Gaspé current, respectively. They showed that the length scales and growth rate of the baroclinic instability predicted by this model were in agreement with studies using sophisticated primitive-equation models and observations. Specifically, the model was able to capture the filamentation and eddy formation associated with the front.

It should be noted that since the single-layer formulation of the weak- β model has been illustrated to only allow for instability when the frontal profile is non-monotonic (see Swaters 1993*b* and Part 1), these instabilities are necessarily baroclinic in nature. Barotropic instabilities do exist as in Part 1. These instabilities are discussed in Reszka & Swaters (1999*a*), where it was illustrated that the breakup of a coupled front into a series of eddies is similar to that of the one-layer model (see Pavia 1992) and compare well with the laboratory results of Griffiths *et al.* (1982). In contrast to the barotropic eddies formed with the strong- β model in Part 1, the eddies do not propagate westward emphasizing the weak effect of the β -plane.

5.3. General model

As discussed previously, the difficulty with the equal-layers model is that the instability results in energy cascading to scales that are smaller than the model resolves. This difficulty extends to all the asymptotic models, specifically the weak- β model discussed in Benilov & Cushman-Roisin (1994), where the nonlinear frontal terms are not included in the baroclinic equation. On the other hand, the thin-upper-layer model is only strictly applicable in situations where $\delta \sim \epsilon^2$, requiring either a very thin front or a large Rossby number. Most observed fronts tend to fall in between these two limits (see Benilov & Reznik 1996) and therefore share characteristics of both these models.

If we examine the general baroclinic equation (2.2), we see that the nonlinear frontal term is $O(\nu)$ smaller than the time-derivative term and the barotropic–baroclinic coupling term. But, with small scales these terms are important as the fourth-order derivatives become large. If the Rossby number is not prohibitively small, the frontal term will affect the evolution of the flow. We expect that this term inhibits unstable growth at small scales since the thin-upper-layer model has a high-wavenumber cutoff for instabilities.

In order to examine the effect of including the frontal terms in the baroclinic equation, we run large-Rossby-number simulations, $\epsilon = 0.25$, of the general weak- β model, (2.1) and (2.2), while varying the depth ratio, $0.1 \leq \delta \leq 1$. Since the Rossby number, ϵ , and hence ν , are no longer taken to be infinitesimal, the nonlinear frontal terms are included in the baroclinic equation. Our goal is to demonstrate that large-scale structures will develop with a thick upper layer if the smaller scales are stabilized by the nonlinear frontal terms. As well, we can clearly illustrate the effect of increasing the frontal depth on the length scales and growth rates of the baroclinic waves.

In figure 3, we present the results of a simulation with $\delta = 0.25$. As in the previous section, waves of large length scale grow rapidly resulting in large meanders of a concentrated current. These meanders tend to break backwards often entrapping colder lower-layer water as a cold-core eddy or pinching off as a warm core eddy. The waves are coupled with cyclonic and anticyclonic eddies in the barotropic flow,

though the cyclonic motion dominates. As well, filaments of lighter fluid extend outward from the front while intrusions of lower-layer fluid (seen as a vanishing of upper-layer depth) reach across the front to the far channel wall. Once again, the current is intensified even though the mean frontal gradient is reduced.

For westward flows, the front evolution shown in figure 3 was typical for all depth ratios. In different simulations, with different initial perturbations, we see different combinations of cold-core eddies, warm-core eddies and filaments. Three things are always common: the front is always very unstable, the current is intensified and the structures in the upper layer are always coupled to strong large-scale eddies in the barotropic stream function. However, for larger depth ratios these structures tend to be unstable and the fronts remain dynamic after eddies have formed. For smaller depth ratios, the waves tend to be of larger scale, the eddies tend to be better defined, and the small-scale noisiness is not a feature.

As before, we only see a release of available PE when the large-scale meanders and eddies form. While the perturbation KE grows throughout the run, this growth does not come at the expense of mean KE or PE. This form of instability, where large growth in the wave energy occurs but apparently not at the expense of mean energy, is discussed in relation to frontal disturbances in Barth (1989*b*). Once again, this illustrates a difference between the LAG limit and the QG limit. In the QG limit, instabilities grow as PE is transferred to KE. In the LAG limit, baroclinic and barotropic kinetic energies must grow concurrently, as required by the conservation of \mathcal{E} , but are not directly tied to a release of PE.

In figure 4, we compare the dimensional wavelengths (*a*) and e-folding times (*b*) of the most unstable waves for various depth ratios for westward flows. Surprisingly, the wavelength varies little, remaining close to 125 km, decreasing slightly as the depth ratio becomes very small. The dashed line plotted is the initial width of the current and is effectively the meridional length scale of the baroclinic wave. The most unstable wavelength is essentially greater than or equal to the current width and the ratio of the zonal wavelength to the meridional length scale increases as the depth ratio decreases. The e-folding time increases exponentially with decreasing depth ratio. This indicates that the large store of energy in a deep front can feed a rapidly growing instability. Barth (1994) has shown that increasing the depth ratio and increasing the β -plane effect both lead to a shift toward a higher-growth-rate smaller-scale instability.

These results are not symmetrical for eastward flows. As noted in §4, eastward flows may be either linearly or nonlinearly stabilized when the depth ratio is small. When the simulations above were repeated for an eastward flow, this asymmetry was apparent as the depth ratio decreased. For large depth ratios, $\delta > 0.35$, the evolution of the front was virtually identical to that for westward flows described above. For $0.35 > \delta > 0.1$, baroclinic waves did grow, but at a much slower rate than for the analogous westward flow. These waves reached a finite amplitude which was then periodically modulated never producing the filamentation and eddies seen for westward flows. For $\delta < 0.1$, the fronts were stable to all perturbations.

It should be noted that these simulations reflect the results of the finite-amplitude analysis of §3.4 and §4.4. There, it was found that nonlinear effects should result in periodic modulation of linear growth when zonal scales are smaller than meridional scales and explosive growth when zonal scales exceed or are similar to meridional scales. In the simulations the vigorous instabilities and eddy formation can be connected to explosive growth. If we examine figure 2 and figure 3, especially the barotropic stream function plots, one concludes that for the large-growth instabilities

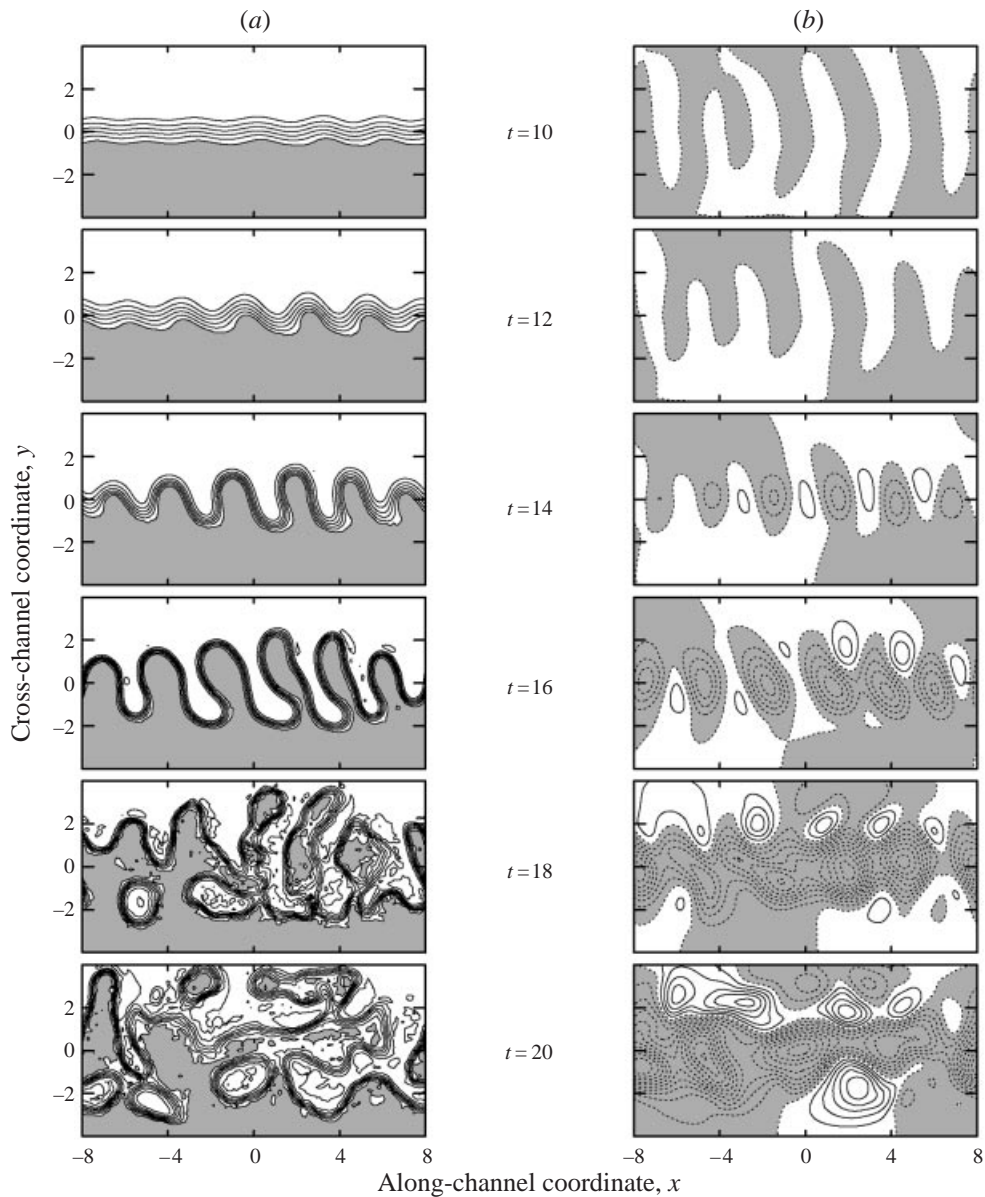


FIGURE 3. Results of the numerical simulation of the general weak- β model with $\delta = \varepsilon = 0.25$. (a) The contours of the upper-layer height and (b) the contours of the barotropic stream function with the contours as in figure 2.

zonal scales are equal to meridional scales. For eastward flows with small depth ratios we see the nonlinear suppression of linear growth at all scales as predicted in §4.4. However, with the different geometry of the front, it is difficult to get a clear picture of the nonlinear effects. Therefore, we ran a simulation with a sloping front extending across a channel. In figure 5, we plot the amplitude of various zonal wavelengths versus time. It is clear that the shorter wavelengths have their growth modulated, developing a quasi-periodic oscillation. On the other hand, longer wavelengths continue to grow throughout the simulation. The growth rate does decrease after an initial

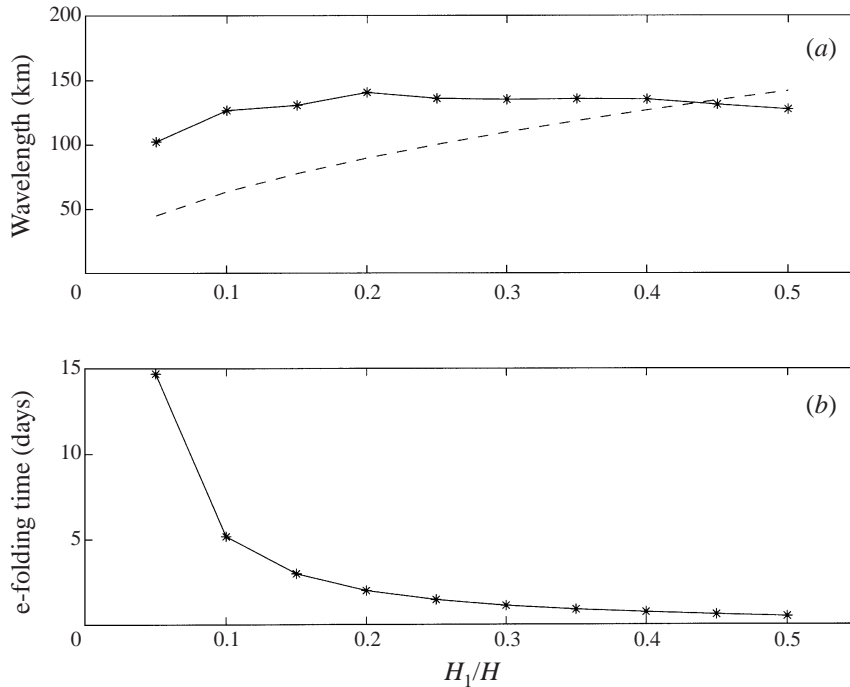


FIGURE 4. The wavelength (a) and the e-folding time (b) of the most unstable mode versus the depth ratio. The dashed line in (a) is the width of the current.

steepening. Thus, as we argued previously, the predicted explosive nonlinear growth is modulated as the wave becomes fully nonlinear, allowing a relatively constant growth rate.

6. Conclusions

We begin by briefly discussing the balances in baroclinic and barotropic equations in the LAG models (see Part 1, for more details). If the β -effect is strong, the barotropic equation is dominated by it and we have the strong- β models discussed in Part 1. However, if this effect is smaller and balances the size of the relative vorticity terms, the barotropic equation becomes a balance between the QG-like evolution of the barotropic flow and the LAG evolution of the baroclinic flow. As the depth ratio increases, the coupling between the two layers becomes more important and dominates the frontal effects. In general, QG models are subject to instability which strives to destroy baroclinic motions (Tang & Cushman-Roisin 1992) and gives rise to large-scale baroclinic waves. Strongly coupled models are also unstable, with the possibility of ultraviolet catastrophe (de Verdière 1986). This is reasonable because increasing the depth ratio increases the vertical scale of the front and thus increases the available energy stored in the front. On the other hand, frontal effects tend to steepen the front favouring the formation of robust, coherent structures (see Cushman-Roisin & Tang 1990 and Tang & Cushman-Roisin 1992) and can be classified as stabilizing. In summary, we expect the weak- β models to be subject to instabilities which will tend to smaller scales at large depth ratios and larger scales at smaller depth ratios. Indeed, it is worthwhile emphasizing that the instability is dependent on the QG instability in the barotropic equation. That is, if we consider the uncoupled limit, we

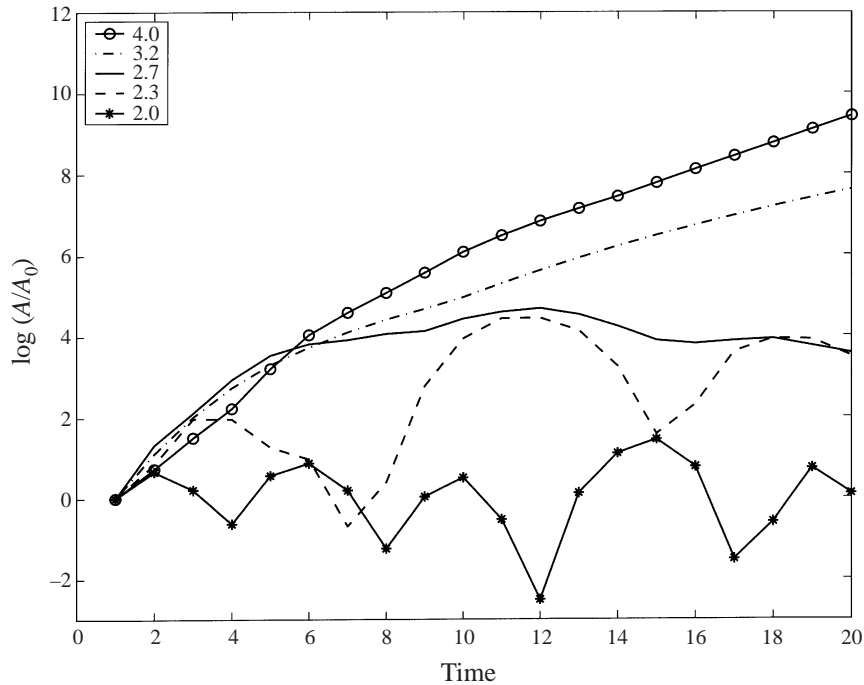


FIGURE 5. Plots of the exponential growth at different wavelengths. For each wavelength, we plot $\log(A/A_0)$ versus time, where A is the wave's amplitude at the given time and A_0 is the wave's initial amplitude. The wavelengths are given in the legend.

find linear instability and results similar to that described in Part 1 (see Slomp & Swaters 1997).

In this paper, we have set out to explore the highly nonlinear nature of these balances. We have concluded that changing the depth ratio, and thus the coupling of the two layers, does change the flow evolution. The equal-layers model is dominated by its strongly coupled baroclinic equation. This leads to ultraviolet catastrophe, large unstable growth at small scales. The balance of terms in the barotropic equation does not suppress this growth because the barotropic relative vorticity terms and the baroclinic LAG terms grow concurrently. Energy considerations do not rule out this growth, as the pseudo-energy invariant \mathcal{E} requires equivalent growth in both the barotropic and baroclinic KE. The nonlinear stability analysis was unable to establish stability conditions as it was not possible to bound growth at small scales. Furthermore, the finite-amplitude instability analysis suggests that waves are subject to an explosive instability when zonal scales exceed meridional scales. As expected, we see the ultraviolet catastrophe in the numerical simulations, with instabilities growing at the smallest scales possible. We conclude that the equal-layers model, which does not include the baroclinic frontal terms at leading order, is unsuited for frontal analysis.

As the depth ratio decreases, the baroclinic equation includes the frontal terms at leading order. The QG-LAG balance in the barotropic equation allows the possibility of instability at the large scales QG dynamics favours and now the baroclinic equation also favours larger scales. This is seen in the linear analysis which predicts instability for a finite band of wavenumbers. The finite-amplitude analysis suggests a suppression instabilities at small zonal scales but explosive nonlinear instability at large zonal

scales. We suggest that it is this explosive nonlinear growth that leads to the coherent eddy formation seen in the numerical solutions of Reszka & Swaters (1999a) and § 5. However, this unstable growth is only found for westward flows, and eastward flows are, in general, much more stable. The similarity of analytical result for the equal-layers and thin-upper-layer limits lead to the conclusion that the results discussed previously in Swaters (1993b) and Reszka & Swaters (1999a) for the thin-upper-layer model extend well beyond the restrictive depth-ratio scaling assumed in the asymptotic derivation. Since the nonlinear growth of waves occurs in both models but not in the QG limit, we conclude that it is the balance of the barotropic relative vorticity advection and the nonlinear, baroclinic advection of momentum *and* mass that allows such growth.

Numerical simulations of the general weak- β model illustrate that frontal terms in the baroclinic equations can suppress small-scale growth for all depth ratios. The result is a concentrated current which develops large-scale structures within a highly unstable front. These large-scale structures were able to release mean PE from the front. The length scale of these structures is relatively constant for all depth ratios, though the growth rate decreases rapidly as the depth ratio decreases. The asymmetry between eastward and westward flows is enhanced as the depth ratio decreases as the β -plane stabilizes thin eastward currents. The vigorously growing instabilities of the isolated front are indicative of the rapidly growing meanders, eddies and squirts common to coastal currents (Paldor & Ghil 1991) and are similar to those shown in the primitive-equation models of Haidvogel *et al.* (1991), Spall (1995), Barth (1994) and Bush *et al.* (1996) and the multi-mode, continuously-stratified QG models of Flierl *et al.* (1987) and Feliks & Ghil (1996). These similarities lead us to the conclusion that despite their simplicity, the two-layer LAG models are capturing the essential physical process involved in frontal instability: the balance of baroclinically unstable QG evolution of the barotropic flow with the highly nonlinear frontal effects which favour large scales.

The analysis of different depth ratios allow us to draw important conclusions about frontal instability. If frontal effects are important, as in the thin-upper-layer model, we see stable anticyclonic eddies form. However, if baroclinic instability dominates frontal effects, as in the equal-layers model, we see the destruction of large-scale features by small-scale instability. The numerical simulations illustrated that if the frontal effects are included in the leading-order dynamics, that is, in the baroclinic equation, they can suppress baroclinic instability at small scales for all depth ratios. As well, we have illustrated that the growth rate of instabilities increases as the depth ratio increases. This favours the growth of anticyclonic eddies as they are regions of local increases in the frontal depth. Together these two features explain why in the LAG regime the geostrophic-turbulence cascade to larger scales is arrested and the final state dominated by stable, anticyclonic eddies with length scales several times the deformation (Tang & Cushman-Roisin 1992).

It is also interesting to compare the results of the two-layer LAG models to the analysis of the Swaters (1991) model (see the Appendix for the model equations). As shown in Karsten & Swaters (1999), the Swaters (1991) model is derived in the LAG limit when considering bottom-trapped flow over topography. Despite being derived in the large-amplitude limit, the nonlinear frontal terms seen in the other LAG models do not appear in the leading-order equations (they are small compared to the strong effect of topography on the baroclinic flow). Due to its simplicity, the Swaters (1991) model allows a richer variety of theoretical analyses (see Swaters 1991, 1993a; Mooney & Swaters 1996; Poulin & Swaters 1999a-c; Karsten, Swaters & Thompson

1995; Karsten & Swaters 1996a; and Swaters 1998a,b). Similarly, the equal-layers and thin-upper-layer models also have corresponding forms for such flows provided the topography is scaled appropriately. The analysis presented here changes very little when bottom topography is included (or even replaces the β -plane) with the results qualitatively the same (see the Appendix).

A couple of important differences arise between the results of the Swaters (1991) model and the models discussed here. The predominant difference is that the strong bottom topography in the Swaters (1991, 1993a) model allows a release of PE that drives the instability (see the discussion in Swaters 1993b). Thus, the instability is asymmetric and is seen as a slumping of fluid down the sloping bottom. The fact that the barotropic motion is primarily QG-like means that this instability occurs for a finite band of length scales and we do not see the ultraviolet catastrophe of the equal-layers model. The finite-amplitude analysis of the Swaters (1991) model illustrates that nonlinear terms suppress the linear growth (Mooney & Swaters 1996) at all scales. This effect can be clearly seen in the numerical simulations of a coupled front in Swaters (1998a) where linear instabilities grow to form filaments that then roll up into eddy-like structures. This instability is fundamentally different from the instability seen in the two-layer LAG models examined here. The instability that develops in the two-layer LAG models examined here is symmetric as PE is not released by simple movement of fluid down a sloping bottom. PE can be released, but this requires the formation of large-scale structures involving a large growth in the KE and a steepening of the front. Eddies form not as a result of a roll-up of filaments but as the growth and pinch off of a single wave. This eddy formation is present in both coupled and isolated fronts for the thin-upper-layer and equal-layers models (Reszka & Swaters 1999 and Karsten 1998). Again this emphasizes that it is the explosive nonlinear growth, predicted in the finite-amplitude analysis for the weak- β models, that leads to the coherent eddy formation seen in the numerical solutions of Reszka & Swaters (1999a) and this paper.

Reszka & Swaters (1999a,b) included a detailed comparison of their thin-upper-layer analysis to the Californian Current and the Gaspé Current, respectively. The model qualitatively captured the explosive instability of the Californian Current and the modulated instability of the Gaspé Current, illustrating the varying effects of bottom topography. Quantitatively, the model did remarkably well in predicting length scales and growth rates of the instabilities. However, it could be argued that they had pushed the thin-upper-layer model beyond its strict regime of applicability by examining fronts with relatively large depth ratios. Our analysis indicates that their results can be extended to large depth ratios with little change qualitatively and only an increase in the growth rate, quantitatively. This suggests that detailed comparison and analysis of a wide variety of fronts and currents could be carried out.

Although we have attempted to examine a number of the aspects of the nonlinear dynamics of weak- β LAG models, there still remain many open areas of research. Further examination of the linear weak- β models using numerical techniques could provide a more accurate picture of the form of the instability that develops on coupled and isolated fronts. Another obvious extension of this work is the examination of several-layer models and an examination of the general geostrophic equations that contain both the LAG and QG limits (see Cushman-Roisin & Tang 1990; Cushman-Roisin *et al.* 1992; and Benilov & Reznik 1996).

Another area of interest is that of eddy development and pinch off. As we have

shown, eddy pinch off occurs from the growth of a single wave, which the meanders to pinch itself off, without friction. This should be compared to the numerical results of Feliks & Ghil (1996). They demonstrated that a continuously stratified QG model could be used to examine the process of eddy pinch off if sufficient vertical modes were included; at least three vertical modes were required to model eddy detachment of a narrow swift current, two modes for a wide slow current. Once again, they note the unrealistic symmetry of cyclonic and anticyclonic eddies obtained with QG models. LAG models, by allowing large isopycnal deflections effectively break this symmetry. Our analysis indicates that the two-layer LAG model can model the eddy pinch off process, but it would require the extension to a continuously stratified LAG model to directly compare results.

Finally, LAG models could be used to estimate the mixing and transport that occurs as a front destabilizes leading to improved eddy parametrization schemes. In Greatbatch (1998), it is proposed that the parametrization of the eddy flux of PV be derived from a PV equation averaged over the thickness between isopycnals. The LAG models studied here allow the simple two-layer analogue of this equation to be studied both analytically and numerically. As well, the LAG models allow measurements of the inertial terms associated with the frontal effects not present in analysis based on a QG assumption. Alternatively, knowledge of two-layer LAG models could be used to include schemes to resolve the necessary scales needed to model frontal instabilities with limited vertical resolution. Further work continues in these areas, and the results will doubtlessly prove very interesting.

Appendix. Adding bottom topography

In this Appendix, we briefly present the changes to the models and analyses if bottom topography is included. The details of two-layer LAG model derivation including bottom topography are given in Karsten & Swaters (1999). Here we simply present the resulting equations with the appropriately scaled bottom topography $h_B(x, y)$.

For the equal-layers model, we scale the bottom topography similarly to the β -plane effect and the model equations become

$$\Delta\psi_t + J(\psi, \Delta\psi) + \beta\psi_x - J\left(h_B, \psi - \frac{\mu}{2}h^2\right) + \mu J[h, h(1 - \mu h)\Delta h + \frac{1}{2}(1 - 2\mu h)|\nabla h|^2] = 0,$$

$$h_t + J(\psi, h) = 0,$$

respectively. As one might expect when the layer depths are equal and the scale amplitude of the bottom topography relatively small, the contribution from the bottom topography only appears in the barotropic equation.

In order to compare the effects of bottom topography to β -plane effects we consider linearly sloping topography $h_B(y) = sy$, where s is the slope of the topography, giving

$$-J\left(h_B, \psi - \frac{\mu}{2}h^2\right) = s(\psi_x - \mu h h_x).$$

The first term on the right-hand-side of this equation is identical to the β -plane effect on the barotropic stream function. The second term results from the fact that the two layers do not feel the bottom topography equally. The changes in the analysis are all a result of this second term and are minor. One thing to note is that the transformation (3.4) can no longer be used to simplify the equations.

If we consider the linear analysis of the gently sloping front with the bottom topography appropriately scaled $s = \Delta\tilde{s}$, the dispersion relationship becomes

$$\tilde{c}(k, \ell) = \frac{-\tilde{\beta} + \tilde{s} \pm \sqrt{(\tilde{\beta} + \tilde{s})^2 - 4\mu K^2[(1 - \mu)\tilde{\alpha}^2 K^2 - \tilde{\alpha}\tilde{s}]}}{2K^2}.$$

Fronts remain unstable to small-scale perturbations and bottom topography stabilizes the front as it becomes large. The final term in the square root indicates that bottom topography has a greater stabilizing influence when the frontal slope and the bottom slope have the same sign. Thus the symmetry of eastward and westward flows has been broken by the topography.

The effect on the nonlinear analysis is minimal. The change in the dispersion relation shifts the marginal stability curves, but this has only a quantitative effect on the final results. The additional term in the equations only affects the spatial variation term in the envelope equation and thus has no effect on nonlinear unstable growth.

For the thin-upper-layer model the effect of bottom topography is again similar to the β -plane effect. There is an additional change as the inclusion of bottom topography breaks the vertical symmetry of the model geometry. While this does not affect the analysis when the two layers are scaled equally, it does when one layer is thinner than the other (see Karsten & Swaters 1999). If we assume the upper layer is thin, as was done in the body of the paper, the model equations reduce to

$$\Delta\psi_t + J(\psi, \Delta\psi) + \beta\psi_x + \mu J(h, h\Delta h + \frac{1}{2}|\nabla h|^2) - J(h_B, \psi) = 0,$$

$$h_t + J(\psi, h) - J(h, h\Delta h + \frac{1}{2}|\nabla h|^2) = 0.$$

In the case of linear bottom topography, $-J(h_B, \psi) = s\psi_x$, and the effect of bottom topography is identical to the β -plane effect (hence the analysis of Reszka & Swaters (1999a) can be applied equally well to a β -plane as discussed in the body of this paper). It should be noted that steep nonlinear bottom topography can destabilize a current if it slopes in the opposite direction to the front (see Reszka & Swaters 1999b).

An analogous model can be derived when the lower layer is thinner. The bottom topography must be very weak as strong bottom topography can dominate the flow in a thin lower layer and result in different dynamics (see below). The model becomes

$$\Delta\psi_t + J(\psi, \Delta\psi) + \beta\psi_x + \mu J(h, h\Delta h + \frac{1}{2}|\nabla h|^2) - J(h_B, h) = 0,$$

$$h_t + J(\psi, h) - J(h, h\Delta h + \frac{1}{2}|\nabla h|^2) + \frac{1}{\mu}J(h_B, h) = 0,$$

where h is now the depth of the lower layer. The bottom topography directly affects the baroclinic flow of the lower layer. The effect of the topography is no longer equivalent to the β -plane effect. The analysis of the model does not differ greatly. Topography stabilizes when it slopes in the same direction as the front but can destabilize the flow if it slopes in the opposite direction. The topography does not affect the nonlinear analysis as it enters the equations only through linear terms. As such, the results of this paper can be extended to the modelling of thin bottom-trapped currents over very weak bottom topography.

The study of thin-lower-layer flows over weak bottom topography leads to a comparison of the models discussed here to the model of Swaters (1991). As discussed in Karsten & Swaters (1999), this model is also a two-layer LAG model in that large isopycnal deflections are allowed. However, the effects of the bottom topography

are scaled equivalently to the baroclinic flow. This allows the bottom topography to strongly influence the baroclinic flow to the extent that the nonlinear frontal terms do not enter the model equations. An appropriately scaled β -plane can be included in the model giving the model equations

$$\Delta\psi_t + J(\psi, \Delta\psi) + \beta\psi_x - J(h_B, \psi + h) = 0,$$

$$\mu h_t + \mu J(\psi, h) + J(h_B, h) = 0.$$

Analysis of this model (with $\beta = 0$) can be found in Swaters (1991, 1993*a*, 1998*a, b*), Karsten & Swaters (1996*a*), Karsten *et al.* (1995), and Mooney & Swaters (1996).

A final note on bottom topography. The above models have been presented with both bottom topography and β -effects but are equally valid on smaller scales where β -effects are small (the model equations are simply the above equations with $\beta = 0$). If the β -effect is not being included in the model, the coordinate system no longer has a fixed direction. As such, the models can be used to examine coastal fronts and bottom-trapped currents following continental shelves.

We would like to thank Mr Matt Reszka for many enjoyable hours discussing this research. Our thanks to Eugene Benilov and an anonymous referee whose suggestions greatly improved the final text. Preparation of this paper was supported in part by Natural Sciences and Engineering Research Council (NSERC) of Canada Research Grants awarded to G. E. S. and an NSERC Postgraduate Scholarship, Killam Doctoral Fellowship and a NSERC Postdoctoral Fellowship awarded to R. H. K.

REFERENCES

- ARAKAWA, A. 1966 Computational design for long term numerical integration of the equations of fluid motion: two-dimensional incompressible flow. *J. Comput. Phys.* **1**, 119–143.
- BARTH, J. A. 1989*a* Stability of a coastal upwelling front. 1. Model development and a stability theorem. *J. Geophys. Res.* **94**, 10844–10856.
- BARTH, J. A. 1989*b* Stability of a coastal upwelling front. 2. Model results and comparison with observations. *J. Geophys. Res.* **94**, 10857–10883.
- BARTH, J. A. 1994 Short-wavelength instabilities on coastal jets and fronts. *J. Geophys. Res.* **99**, 16095–16115.
- BENILOV, E. S. 1992 Large-amplitude geostrophic dynamics: the two layer model. *Geophys. Astrophys. Fluid Dyn.* **66**, 67–79.
- BENILOV, E. S. 1993 Baroclinic instability of large-amplitude geostrophic flows. *J. Fluid Mech.* **251**, 501–514.
- BENILOV, E. S. 1994 Dynamics of large-amplitude geostrophic flows: the case of ‘strong’ beta-effect. *J. Fluid Mech.* **262**, 157–169.
- BENILOV, E. S. 1995 On the stability of large-amplitude geostrophic flows: the case of ‘strong’ beta effect. *J. Fluid Mech.* **284**, 137–158.
- BENILOV, E. S. & CUSHMAN-ROISIN, B. 1994 On the stability of two-layered large-amplitude geostrophic flows with thin upper layer. *Geophys. Astrophys. Fluid Dyn.* **76**, 29–41.
- BENILOV, E. S. & REZNIK, G. M. 1996 The complete classification of large-amplitude geostrophic flows in a two layer fluid. *Geophys. Astrophys. Fluid Dyn.* **82**, 1–22.
- BOSS, E., PALDOR, N. & THOMPSON, L. 1996 Stability of a potential vorticity front from quasi-geostrophy to shallow water. *J. Fluid Mech.* **315**, 65–84.
- BUSH, A. B. G., MCWILLIAMS, J. C. & PELTIER, W. R. 1995 The formation of eddies in symmetric and asymmetric jets. Part 1: Early time development and bulk eddy transports. *J. Phys. Oceanogr.* **25**, 1959–1979.
- BUSH, A. B. G., MCWILLIAMS, J. C. & PELTIER, W. R. 1996 The formation of eddies in symmetric and asymmetric jets. Part 2: Late time evolution and coherent vortex formation. *J. Phys. Oceanogr.* **26**, 1825–1848.

- CHARNEY, J. G. & FLIERL, G. R. 1981 Oceanic analogues of large-scale atmospheric motions. In *Evolutions of Physical Oceanography* (ed. B. A. Warren & C. Wunsch), pp. 504–548. The MIT Press.
- CHASSIGNET, E. P. & CUSHMAN-ROISIN, B. 1991 On the influence of a lower layer on the propagation of nonlinear oceanic eddies. *J. Phys. Oceanogr.* **21**, 939–957.
- CUSHMAN-ROISIN, B. 1986 Frontal geostrophic dynamics. *J. Phys. Oceanogr.* **16**, 132–143.
- CUSHMAN-ROISIN, B., SUTYRIN, G. G. & TANG, B. 1992 Two-layer geostrophic dynamics. Part I: Governing equations. *J. Phys. Oceanogr.* **22**, 117–127.
- CUSHMAN-ROISIN, B. & TANG, B. 1990 Geostrophic turbulence and the emergence of eddies beyond the radius of deformation. *J. Phys. Oceanogr.* **20**, 97–113.
- DRAZIN, P. G. & REID, W. H. 1981 *Hydrodynamic Stability*. Cambridge University Press.
- FELIKS, Y. & GHIL, M. 1996 Mixed barotropic–baroclinic eddies growing on an eastward jet. *Geophys. Astrophys. Fluid Dyn.* **82**, 137–171.
- FLIERL, G. R., MALANOTTE-RIZZOLI & ZABUSKY, N. J. 1987 Nonlinear waves and coherent vortex structures in barotropic β -plane jets. *J. Phys. Oceanogr.* **17**, 1408–1438.
- GHIL, M. & PALDOR, N. 1994 A model equation for nonlinear wavelength selection and amplitude evolution of frontal waves. *J. Nonlinear Sci.* **4**, 471–496.
- GREATBATCH, R. J. 1998 Exploring the relationship between eddy-induced transport velocity, vertical momentum transfer, and the isopycnal flux of potential vorticity. *J. Phys. Oceanogr.* **28**, 422–432.
- GRIFFITHS, R. W., KILLWORTH, P. D. & STERN, M. E. 1982 Ageostrophic instability of ocean currents. *J. Fluid Mech.* **117**, 343–377.
- GRIFFITHS, R. W. & LINDEN, P. F. 1981 The stability of buoyancy-driven coastal currents. *Dyn. Atmos. Oceans* **5**, 281–306.
- HAIDVOGEL, D. B., BECKMAN, A. & HEDSTROM, K. S. 1991 Dynamical simulations of filament formation and evolution in the coastal transition zone. *J. Geophys. Res.* **96**, 15017–15040.
- IKEDA, M. & EMERY, W. J. 1984 Satellite observations and modelling of meanders in the California current system off Oregon and Northern California. *J. Phys. Oceanogr.* **14**, 1434–1450.
- IKEDA, M., EMERY, W. J. & MYSAK, L. A. 1984 Seasonal variability in meanders of the California current system off Vancouver Island. *J. Geophys. Res.* **89**, 3487–3505.
- KARSTEN, R. H. 1998 Nonlinear effects in two-layer, frontal-geostrophic models of surface ocean fronts. PhD thesis, Department of Mathematical Sciences, University of Alberta.
- KARSTEN, R. H. & SWATERS, G. E. 1996a Nonlinear stability of baroclinic fronts in a channel with variable topography. *Stud. Appl. Maths* **96**, 183–199.
- KARSTEN, R. H. & SWATERS, G. E. 1996b A note on the stability theory of buoyancy-driven ocean currents over a sloping bottom. *Z. Angew. Math. Phys.* **47**, 28–38.
- KARSTEN, R. H. & SWATERS, G. E. 1999 A unified asymptotic derivation of two-layer, frontal geostrophic models including planetary sphericity and variable topography. *Phys. Fluids* **11**, 2583–2597.
- KARSTEN, R. H. & SWATERS, G. E. 2000 Nonlinear effects in two-layer large-amplitude geostrophic dynamics. Part I. The strong-beta case. *J. Fluid Mech.* **412**, 125–160.
- KARSTEN, R. H., SWATERS, G. E. & THOMSON, R. E. 1995 Stability characteristics of deep-water replacement in the Strait of Georgia. *J. Phys. Oceanogr.* **25**, 2391–2403.
- KILLWORTH, P. D. 1983 Long wave instability of an isolated front. *Geophys. Astrophys. Fluid Dyn.* **25**, 235–258.
- KILLWORTH, P. D., PALDOR, N. & STERN, M. E. 1984 Wave propagation and growth on a surface front in a two-layer geostrophic current. *J. Mar. Res.* **42**, 761–785.
- KILLWORTH, P. D. & STERN, M. E. 1982 Instabilities on density-driven boundary currents and fronts. *Geophys. Astrophys. Fluid Dyn.* **22**, 1–28.
- MCCREARY, J. P., FUKAMACHI, Y. & KUNDU, P. K. 1991 A numerical investigation of jets and eddies near an eastern ocean boundary. *J. Geophys. Res.* **96**, 2525–2534.
- MOONEY, C. J. & SWATERS, G. E. 1996 Finite amplitude baroclinic instability of a mesoscale gravity current in a channel. *Geophys. Astrophys. Fluid Dyn.* **82**, 173–205.
- OLSON, D. B., SCHMITT, R. W., KENNELLY, M. & JOYCE, T. M. 1985 A two layer diagnostic model of the long-term physical evolution of warm core ring 82B. *J. Geophys. Res.* **90**, 8813–8822.
- PALDOR, N. 1983a Linear stability and stable modes of geostrophic fronts. *Geophys. Astrophys. Fluid Dyn.* **24**, 299–326.

- PALDOR, N. 1983*b* Stability and stable modes of coastal fronts. *Geophys. Astrophys. Fluid Dyn.* **27**, 217–228.
- PALDOR, N. 1987 Nonlinear waves on a coupled density front. *Geophys. Astrophys. Fluid Dyn.* **37**, 171–191.
- PALDOR, N. & GHIL, M. 1990 Finite-wavelength instabilities of a coupled density front. *J. Phys. Oceanogr.* **20**, 114–123.
- PALDOR, N. & GHIL, M. 1991 Shortwave instabilities of coastal currents. *Geophys. Astrophys. Fluid Dyn.* **58**, 225–241.
- PALDOR, N. & KILLWORTH, P. D. 1987 Instabilities of a two-layer coupled front. *Deep-Sea Res.* **34**, 1525–1539.
- PAVIA, N. 1992 The breakup of frontal filaments. *J. Phys. Oceanogr.* **22**, 399–403.
- PEDLOSKY, J. 1970 Finite amplitude baroclinic waves. *J. Atmos. Sci.* **27**, 15–30.
- PEDLOSKY, J. 1972 Finite amplitude baroclinic wave packets. *J. Atmos. Sci.* **29**, 680–686.
- PEDLOSKY, J. 1982 Finite amplitude baroclinic waves at minimum critical shear. *J. Atmos. Sci.* **39**, 555–562.
- PEDLOSKY, J. 1987 *Geophysical Fluid Dynamics*. Springer.
- PHILLIPS, N. A. 1963 Geostrophic motion. *Rev. Geophys.* **1**, 123–176.
- POULIN, F. J. & SWATERS, G. E. 1999*a* Sub-inertial dynamics of density-driven flows in a continuously stratified fluid on a sloping bottom. I. Model derivation and stability characteristics. *Proc. R. Soc. Lond. A* **455**, 2281–2304.
- POULIN, F. J. & SWATERS, G. E. 1999*b* Sub-inertial dynamics of density-driven flows in a continuously stratified fluid on a sloping bottom. II. Isolated eddies and radiating cold domes. *Proc. R. Soc. Lond. A* **455**, 2305–2329.
- POULIN, F. J. & SWATERS, G. E. 1999*c* Sub-inertial dynamics of density-driven flows in a continuously stratified fluid on a sloping bottom. Part 3. Nonlinear stability theory. *Can. Appl. Maths Q.* **7**, 49–68.
- RESZKA, M. K. 1997 Finite amplitude waves and eddy development on a baroclinically unstable front over a sloping bottom. MSc thesis, Department of Mathematical Sciences, University of Alberta.
- RESZKA, M. K. & SWATERS, G. E. 1999*a* Eddy formation and interaction in a baroclinic frontal geostrophic model. *J. Phys. Oceanogr.* **29**, 3025–3042.
- RESZKA, M. K. & SWATERS, G. E. 1999*b* Numerical investigation of baroclinic instability in the Gaspé Current using a frontal geostrophic model. *J. Geophys. Res.* **104**, 25685–25696.
- ROBINSON, A. R. (ed.) 1983 *Eddies in Marine Science*. Springer.
- RODEN, G. I. 1975 On North Pacific temperature, salinity, sound velocity and density fronts and their relation to the wind energy flux fields. *J. Phys. Oceanogr.* **5**, 557–571.
- SLOMP, C. G. & SWATERS, G. E. 1997 Finite amplitude perturbations and modulational instability of a stable geostrophic front. *Geophys. Astrophys. Fluid Dyn.* **86**, 149–172.
- SPALL, M. A. 1995 Frontogenesis, subduction, and cross front exchange at upper ocean fronts. *J. Geophys. Res.* **100**, 2543–2557.
- STAMMER, D. 1997 Global characteristics of ocean variability from regional TOPEX/POSEIDON altimeter measurements. *J. Phys. Oceanogr.* **27**, 1743–1769.
- SWATERS, G. E. 1991 On the baroclinic instability of cold-core coupled density fronts on a sloping continental shelf. *J. Fluid Mech.* **224**, 361–382.
- SWATERS, G. E. 1993*a* Nonlinear stability of intermediate baroclinic flow on a sloping bottom. *Proc. R. Soc. Lond. A* **442**, 249–272.
- SWATERS, G. E. 1993*b* On the baroclinic dynamics, Hamiltonian formulation and general stability characteristics of density-driven surface currents and fronts over a sloping continental shelf. *Phil. Trans. R. Soc. Lond. A* **345**, 295–325.
- SWATERS, G. E. 1998*a* Numerical simulations of the baroclinic dynamics of density-driven coupled fronts and eddies on a sloping bottom. *J. Geophys. Res.* **103**, 2945–2961.
- SWATERS, G. E. 1998*b* Dynamics of radiating cold domes on a sloping bottom. *J. Fluid Mech.* **364**, 221–251.
- TAN, B. & LIU, S. 1995 Collisions and interactions of solitons in a baroclinic atmosphere. *J. Atmos. Sci.* **52**, 1501–1512.
- TANG, B. & CUSHMAN-ROISIN, B. 1992 Two-layer geostrophic dynamics. Part II: Geostrophic turbulence. *J. Phys. Oceanogr.* **22**, 128–138.

- VERDIERE, A. C. DE 1986 On mean flow instabilities within the planetary geostrophic equations. *J. Phys. Oceanogr.* **16**, 1981–1984.
- VISBECK, M. J., MARSHALL, J., HAINES, T. & SPALL, M. 1997 On the specification of eddy transfer coefficients in coarse resolution ocean circulation models. *J. Phys. Oceanogr.* **27**, 381–402.
- YAMAGATA, T. 1982 On nonlinear planetary waves: a class of solutions missed by the traditional quasigeostrophic approximation. *J. Oceanogr. Soc. Japan* **38**, 236–244.